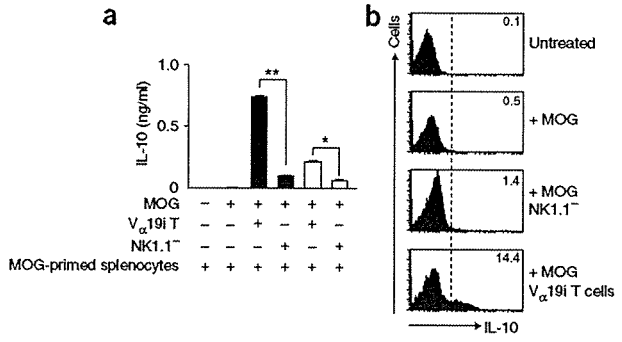

Figure 4 Interactions of V_α19i T cells and splenocytes induce IL-10. (**a**) Cytometric bead assay of IL-10 in the supernatants of liver V_α19i T cells from naive V_α19iTg*Cd1d1*$^{-/-}$ mice, cultured for 72 h with MOG(35–55)-specific splenocytes and MOG(35–55) (filled bars). In some cases, V_α19i T cells were separated from splenocytes by transwell inserts (open bars). Controls received NK1.1$^-$ liver cells from V_α19iTg*Cd1d1*$^{-/-}$ mice. Data represent ± s.e.m. from duplicate samples from three independent experiments. *, $P < 0.01$, and **, $P < 0.001$, compared with control (two-tailed Student's *t*-test). (**b**) Intracellular flow cytometry of IL-10 production by total cells from **a**. Areas to the right of dashed lines indicate positive cellular staining; numbers in histograms indicate percentages of IL-10-producing cells. Data are representative of three separate experiments.

IFN-γ secretion was more susceptible to the inhibitory effects of V_α19i T cells than was IL-17 (**Fig. 3b**). Splenocytes acted like lymph node cells (data not shown).

Overexpression of the V_α19i TCR might compromise the ability of conventional T cells to recognize myelin-derived peptides. However, the proliferative responses of MOG(35–55)-reactive T cells were not lower in V_α19iTg*Cd1d1*$^{-/-}$ mice, despite the inhibition of T_H1 cytokine production (**Fig. 3c**). Therefore, it is unlikely that the degree of EAE suppression seen in V_α19iTg*Cd1d1*$^{-/-}$ mice was the result of alterations in the MOG(35–55)-specific T cell repertoire. However, to exclude that possibility, we did adoptive transfer experiments. We transferred 1×10^6 V_α19i T cells isolated from V_α19iTg*Cd1d1*$^{-/-}$ mice into nontransgenic mice on the day of EAE induction. Mice that received TCRβ$^+$ T cells were significantly protected from EAE (**Fig. 3d**) and the onset of clinical disease was significantly delayed (**Table 1**) compared with that of mice that received V_α19i$^-$ NK1.1$^-$ T cells.

Next we sought to determine if V_α19i T cell deficiency could also influence clinical EAE. As no V_α19i-specific TCR antibody is available to deplete mice of V_α19i T cells *in vivo*, we used *Mr1*$^{-/-}$ mice, which lack V_α19i T cells[7]. As wild-type nontransgenic mice have about four times more V_α14i NKT cells than V_α19i T cells and *Cd1d1*$^{-/-}$mice did not show protection from EAE (**Fig. 2a**), we sought to determine whether the deletion of small numbers of MR1-restricted T cells could alter the clinical course of EAE. Compared with wild-type nontransgenic controls, *Mr1*$^{-/-}$ mice showed a significantly more severe form of EAE with an earlier onset ($P < 0.05$; **Fig. 3e** and **Table 1**). Furthermore, T cells from *Mr1*$^{-/-}$ mice proliferated more and produced more T_H1 cytokines and less IL-10 (data not shown). These experiments collectively suggest that V_α19i T cells have a regulatory function in a T_H1-mediated autoimmune disease.

V_α19i T cells induce B cell IL-10 production

MOG(35–55)-primed V_α19iTg lymph node cells and splenocytes secreted IL-10, which potently inhibits EAE[27–30] (**Fig. 3a**). Therefore, we sought to determine whether an increase in V_α19i T cells augmented general IL-10 production. To address that, we developed a mixed-lymphocyte assay in which we cultured NK1.1$^+$ or NK1.1$^-$ T cells from V_α19iTg*Cd1d1*$^{-/-}$ mice together with MOG(35–55)-primed nontransgenic splenocytes (**Fig. 4a**). Neither NK1.1$^+$ or NK1.1$^-$ T cells inhibited the proliferation of MOG(35–55)-primed splenic T cells restimulated with MOG(35–55) (data not shown). Cytokine analysis showed that the coculture supernatant contained considerable IL-10 (after stimulation with MOG(35–55)) in the presence of NK1.1$^+$ but not NK1.1$^-$ T cells from V_α19iTg*Cd1d1*$^{-/-}$ mice (**Fig. 4a**). NK1.1$^+$ T cells from V_α19iTg*Cd1d1*$^{-/-}$ mice induced IL-10 production even in the absence of MOG(35–55) ($P < 0.05$; **Supplementary Fig. 2** online). However, IL-10 secretion was significantly enhanced in the presence of exogenous MOG(35–55) ($P < 0.01$; **Supplementary Fig. 2**). Intracellular cytokine analysis confirmed that IL-10 production was induced by the addition of NK1.1$^+$ but not NK1.1$^-$ T cells from V_α19iTg*Cd1d1*$^{-/-}$ mice (**Fig. 4b**). However, in the presence of transwell inserts, IL-10 production was inhibited, indicating that V_α19i T cell–mediated IL-10 production depends mainly on cell-cell contact (**Fig. 4a**). IL-4 and IL-5 were below the limit of detection (less than 5 pg/ml), and IFN-γ and TNF were slightly upregulated in the presence of V_α19i T cells (data not shown).

To determine which cells produced IL-10, in the same coculture experiment we analyzed IL-10 production by CD19$^+$, CD4$^+$, CD8$^+$,

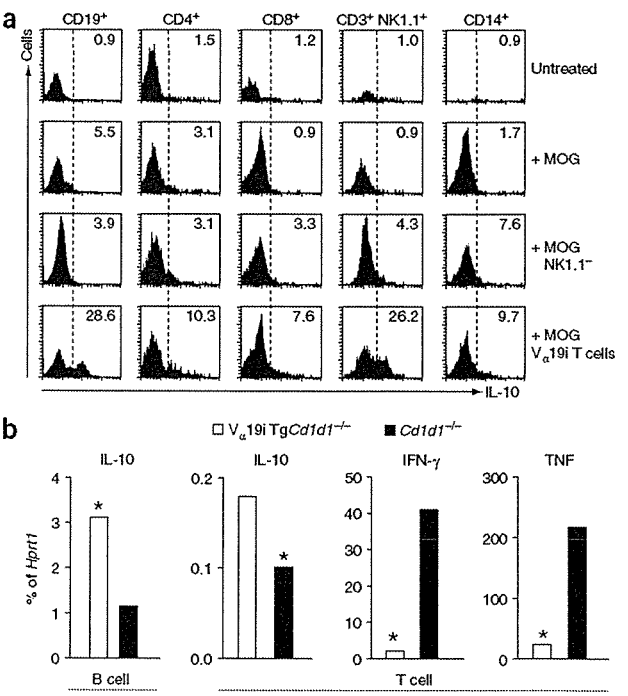

Figure 5 V_α19i T cells induce B cells to secrete IL-10. (**a**) Intracellular flow cytometry of IL-10 production by liver V_α19i T cells from naive V_α19iTg*Cd1d1*$^{-/-}$ mice, cultured for 72 h with MOG(35–55)-specific splenocytes and MOG(35–55). Areas to the right of dashed lines indicate positive cellular staining; numbers in histograms indicate percentage of IL-10-producing cells expressing various surface markers (above plots). Data are representative of two separate experiments. (**b**) Real-time RT-PCR of the expression of transcripts encoding various cytokines (above graphs) by splenic CD19$^+$ B cells or CD4$^+$ T cells sorted from mice with EAE. Data are expressed as a percentage of expression of *Hprt1* and are representative of two separate experiments. *, $P < 0.05$ (two-tailed Student's *t*-test).

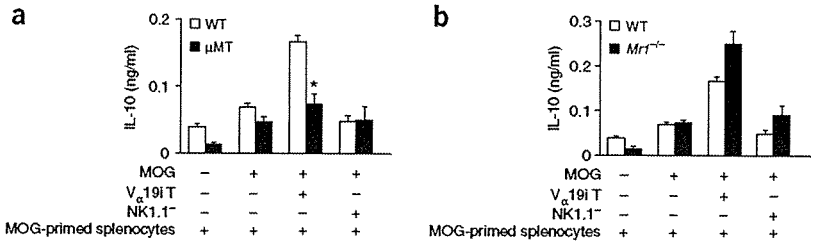

Figure 6 V_α19i T cell–induced IL-10 production is partially B cell dependent but completely MR1 independent. Cytometric bead assay of IL-10 in the supernatants of liver V_α19i T cells from naive V_α19iTg*Cd1d1*$^{-/-}$ mice, cultured for 72 h with MOG(35–55) plus MOG(35–55)-specific splenocytes from wild-type nontransgenic or B cell–deficient μMT mice (**a**) or from wild-type nontransgenic or MR1-deficient mice (**b**). Data represent mean ± s.e.m. of duplicate samples from three independent experiments. *, $P < 0.05$, compared with control (two-tailed Student's *t*-test).

$CD3^+NK1.1^+$ or $CD14^+$ cells using intracellular cytokine flow cytometry. The addition of V_α19i T cells greatly increased IL-10 production by $CD19^+$ B cells and $CD3^+$ $NK1.1^+$ NKT cells (**Fig. 5a**). $CD4^+$ and $CD8^+$ T cells also showed slight increases in IL-10 production in the presence of V_α19i T cells. To demonstrate that B cells were the main IL-10 producing cells *in vivo*, we extracted RNA from sorted splenic $CD4^+$ T cells or $CD19^+$ B cells from V_α19iTg*Cd1d1*$^{-/-}$ or nontransgenic mice with EAE (**Fig. 5b**). In agreement with the results of the *in vitro* coculture system, we found that B cells isolated from V_α19iTg*Cd1d1*$^{-/-}$ mice had higher expression of mRNA transcripts encoding IL-10 than did T cells (**Fig. 5b**). In addition, B cells from V_α19iTg*Cd1d1*$^{-/-}$ mice had higher expression of *Il10* transcripts than did B cells from *Cd1d1*$^{-/-}$ mice (**Fig. 5b**). In contrast, $CD4^+$ T cells from V_α19iTg*Cd1d1*$^{-/-}$ mice had lower expression of T_H1 cytokine–encoding mRNA transcripts than did $CD4^+$ T cells from *Cd1d1*$^{-/-}$ mice (**Fig. 5b**).

To determine if V_α19i T cell–B cell interactions are essential for IL-10 production in the coculture system, we immunized B cell–deficient (μMT) mice with MOG(35–55) to obtain a source of MOG-primed spleen cells lacking B cells. After culture together with V_α19i T cells, B cell–deficient splenocytes produced less IL-10 than did wild-type nontransgenic splenocytes (**Fig. 6a**). As μMT knockout mice may have unusual follicular architecture, to exclude potential indirect effects we repeated these coculture experiments using B cell–depleted wild-type nontransgenic splenocyte samples. B cell–depleted splenocyte samples produced less IL-10 than did nondepleted splenocyte samples whereas the readdition of wild-type B cells to B cell–depleted splenocyte samples restored IL-10 production (56.3 ± 1.2 pg/ml for B cell–depleted splenocyte samples; 126.0 ± 4.4 pg/ml for B cell–depleted splenocyte samples with B cells 'added back'; and 170.4 ± 0.8 pg/ml for nondepleted splenocyte samples).

We hypothesized that an interaction between MR1 on B cells and the V_α19i TCR on T cells could induce IL-10 secretion from both cell types. To test that, we immunized *Mr1*$^{-/-}$ mice with MOG(35–55), followed by coculture experiments. In the absence of MR1, V_α19i T cell–mediated IL-10 production was not reduced (**Fig. 6b**). These results suggest that V_α19i T cell-induced IL-10 production can occur at least in part through MR1-independent interaction with B cells. However, non–B cells also seem to contribute to V_α19i T cell–induced IL-10 production.

Costimulation in V_α19i T cell-induced IL-10 production

Naive V_α19i T cells from V_α19iTg*Cd1d1*$^{-/-}$ mice expressed more of the costimulatory molecules CD278 (ICOS), CD86 (B7-2), CD154 (CD40L) and CD28 than did naive splenic T cells (**Fig. 7a**). V_α19i T cells also expressed CD44 more 'brightly' than did naive T cells (data not shown). These results indicate that V_α19i T cells have an activated or memory phenotype, similar to that of V_α14i NKT cells[1] and 'mucosal-associated invariant T cells' isolated from gut mucosa[2].

Given that MR1 is not required for IL-10 production, we hypothesized that costimulatory interactions may provide the stimulus for IL-10 production. To test that, we repeated the coculture experiments in the presence of blocking antibodies specific for the costimulatory molecules B7RP-1, CD80, CD86 and CD40L. We found that blockade of each costimulatory pathway resulted in significantly lower IL-10 secretion than that of control cocultures treated with control immunoglobulin (**Fig. 7b**). However, blockade of the ICOS–B7RP-1 pathway inhibited IL-10 production most substantially. To extend those

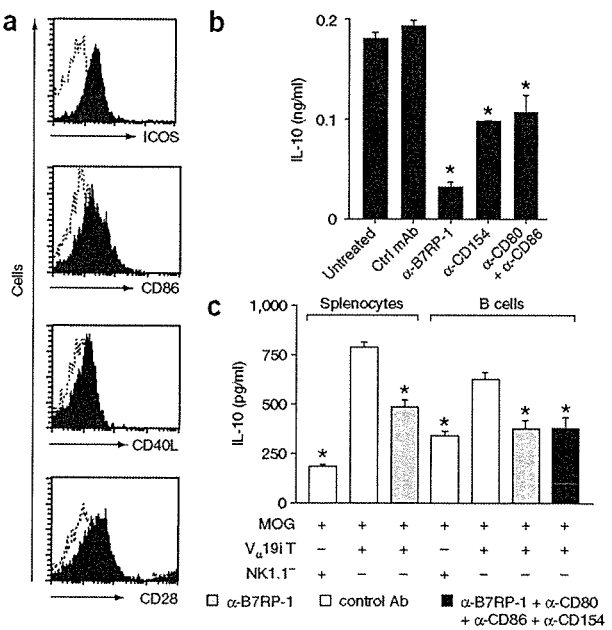

Figure 7 ICOS–B7RP-1 costimulation contributes to V_α19i T cell–induced B cell IL-10 production. (**a**) Flow cytometry of costimulatory molecule expression on the surface of liver V_α19i T cells (filled histograms) and naive splenic T cells from C57BL/6 mice (dotted lines). Data are representative of three separate experiments. (**b**) Cytometric bead assay of IL-10 in the supernatants of liver V_α19i T cells from naive mice, cultured with MOG(35–55) and MOG(35–55)-specific splenocytes from wild-type nontransgenic EAE mice in the presence of isotype-matched control antibody (Ctrl mAb) or of blocking antibodies specific to various costimulatory molecules (α–; below graph), measured after 72 h of incubation. Data are representative of two separate experiments. (**c**) Cytometric bead assay of IL-10 in the supernatants of liver V_α19i T cells from naive V_α19iTg*Cd1d1*$^{-/-}$ mice, cultured with MOG(35–55) and MOG(35–55)-specific splenocytes or sorted B cells from wild-type nontransgenic EAE mice in the presence of various antibodies (key), measured after 72 h of incubation. *, $P < 0.001$, compared with control groups (analysis of variance). Data represent mean ± s.e.m. of triplicate samples from two separate experiments.

findings further, we cultured V_α19i T cells together with purified B cells. This resulted in B7RP-1-dependent IL-10 production (**Fig. 7c**). B7RP-1 blockade partially inhibited IL-10 production in cocultures of V_α19i T cells and splenocytes and fully inhibited IL-10 production in cocultures of V_α19i T cells and purified B cells (**Fig. 7c**). These results suggest that although B cells are a chief producer of IL-10 in this system, other cell types also contribute to V_α19i T cell–induced IL-10 production. Furthermore, the ICOS–B7RP-1 pathway is vital for V_α19i T cell–induced, B cell–mediated IL-10 production, as blockade with a combination of antibodies to costimulatory molecules (B7RP-1, CD80, CD86 and CD40L) inhibited IL-10 to the same degree as anti-B7RP-1 alone (**Fig. 7c**). However, other costimulatory molecules are involved in V_α19i T cell–induced IL-10 production from whole splenocytes (**Fig. 7b**).

DISCUSSION

Although T cells expressing the invariant V_α19-J_α33 TCR chain were first identified in 1993 (ref. 22), knowledge of the immunological function of this invariant T cell population is still limited. Nevertheless, important characteristics of this lymphocyte subset have been characterized, including their restriction by MR1, their TAP (transporter associated with antigen processing)—independent development in rodents, humans and cattle, and the notable interspecies conservation of this invariant TCR. Because CD1d-restricted V_α14i NKT cells, which influence autoimmunity, have similar properties, we speculated that MR1-resricted T cells would also be capable of modifying autoimmunity. However, V_α19i T cells are distinct from V_α14i CD1d-restricted T cells in their 'preferential' distribution in the gut mucosa and their dependence on the presence of B cells and gut flora.

V_α7.2i T cells, the human homolog of V_α19i T cells, are present in lesions of patients with multiple sclerosis[25]. As multiple sclerosis is a demyelinating disease involving autoimmune T cells, B cells, macrophages and various inflammatory mediators, it is possible that MR1-restricted T cells may regulate ongoing disease activity in the CNS. Using an animal model of multiple sclerosis, we examined the effect of overexpression or deletion of MR1-restricted T cells on disease course and severity. Our study suggests that V_α19i T cells can suppress autoimmune inflammation. In addition, we have shown that V_α19i T cells have a memory or activated surface phenotype and are able to produce large amounts of T_H1 and T_H2 cytokines. NK1.1$^+$ T cells from V_α19iTg mice produced more cytokines than did NK1.1$^+$ T cells from V_α19iTg*Cd1d1*$^{-/-}$ mice, indicating a possible interaction between CD1d- and MR1-restricted lymphocytes.

We undertook several approaches to determine whether V_α19i T cells regulate EAE pathogenesis. Overexpression of V_α19i T cells protected mice from clinical EAE. Inhibition of EAE was associated with reduced infiltration and demyelination of the spinal cord as well as a decrease in the production of disease-promoting T_H1 cytokines in the draining lymph nodes and spleen and a reciprocal increase in IL-10, a well established inhibitor of EAE[27–30]. IL-17-secreting cells, which function independently of T_H1 cells, may promote EAE[31]. Here we determined that the inhibitory effect of V_α19i T cells is biased toward prevention of secretion of T_H1 cytokines rather than IL-17.

A potential limitation of TCR-transgenic models is the possible disruption of conventional TCR diversity, which could skew TCR recognition of MOG. However, this is unlikely, as anti-MOG T cell proliferative responses were similar in wild-type nontransgenic and V_α19iTg mice. Furthermore, we adoptively transferred liver V_α19i T cells from naive V_α19iTg*Cd1d1*$^{-/-}$ mice into wild-type nontransgenic mice with EAE, which express natural TCR diversity. In those experiments, V_α19i T cells effectively inhibited EAE, suggesting that V_α19i T cells have a regulatory function during EAE. However, a potential limitation of our model is the difficulty of obtaining pure V_α19i T cell preparations because of the lack of a V_α19 TCR–specific antibody. Therefore, experiments using sorted CD3$^+$ NK1.1$^+$ cells from V_α19iTg*Cd1d1*$^{-/-}$ mice may also contain small numbers of non–V_α14i TCR NK1.1$^+$ T cells of other TCR specificities. To ascertain whether normal numbers of V_α19i T cells in wild-type nontransgenic mice could be involved during EAE, we induced EAE in *Mr1*$^{-/-}$ mice and found that the absence of V_α19i T cells resulted in a more severe clinical disease than that of wild-type nontransgenic mice.

V_α19i T cells most likely exert their main effects in the peripheral lymphoid tissue, as the reduction in proinflammatory cytokines and increase in IL-10 was in the draining lymph nodes and spleen. We also demonstrated that the protective effect of V_α19i T cells was independent of V_α14i NKT cells by using V_α19iTg mice on a CD1d-deficient background. Notably, we found reduced adhesion molecule expression on effector T cells from V_α19iTg*Cd1d1*$^{-/-}$ mice, which correlated with reduced T cell infiltration of the CNS. However, we did note low numbers of V_α19i T cells (CD3$^+$NK1.1$^+$ from V_α19iTg*Cd1d1*$^{-/-}$mice) and B cells in the CNS of mice with EAE, suggesting that V_α19i T cells may also regulate EAE in the CNS.

Coculture experiments suggested that IL-10-producing B cells are involved in the amelioration of EAE in V_α19iTg*Cd1d1*$^{-/-}$ mice. Notably, that finding is consistent with published studies demonstrating that IL-10-producing B cells are involved in spontaneous remission from EAE and could limit clinical disease when adoptively transferred into mice with EAE[32] or a model of collagen-induced arthritis[33]. However, those results do not exclude the possibility that *in vivo*, other cell types are also involved in V_α19i T cell–mediated immune regulation. B cells express MR1 (ref. 34), and V_α19i T cells are MR1 restricted[7], but IL-10 production was unaffected in coculture experiments with lymphocytes from MR1-deficient mice, suggesting that MR1, although necessary for V_α19i T cell selection, is not essential for V_α19i T cell–induced B cell IL-10 production.

T cell activation requires TCR stimulation as well as costimulatory signals. Many costimulatory molecules that regulate cell activation and cytokine secretion have been identified: ICOS and its ligand B7RP-1, CD40-CD40L and CD28-CD80 and CD28-CD86 (refs. 35–38). ICOS costimulation induces IL-10 production as well as help for B cell maturation and CD40L expression[39,40]. The expression of costimulatory molecules on V_α19i T cells was unknown before; we have demonstrated here that V_α19i T cells express ICOS, CD28, CD86 and CD40L. To determine the contribution of each of these costimulatory signaling pathways on the production of IL-10 after V_α19i T cell–B cell interactions, we repeated the coculture experiments using blocking monoclonal antibody to each of the costimulatory pathways. We found that blockade of the ICOS–B7RP-1 pathway inhibited IL-10 production. Furthermore, blockade of the CD40-CD40L, CD28-CD80 or CD28-CD86 pathway also blocked IL-10 production, although not to the extent seen with ICOS blockade.

Commensal flora in the gut are important for the selection of V_α19i T cells[7]. V_α19i T cells may also control gut production of immunoglobulin A from B cells, suggesting involvement of V_α19i T cells in intestinal B cell regulation[7]. Additionally, IL-10 is important for inhibiting excessive inflammation toward gut flora[41], and it has been shown that IL-10 and transforming growth factor-β are involved in immunoglobulin A synthesis and secretion[42]. In the presence of IL-10 and CD40-CD40L signaling, production of immunoglobulin A is increased[43]. Thus, our findings presented here are consistent with the hypothesis that V_α19i T cells are involved in the homeostasis of gut immunity[2,7]. We have shown that V_α19i T cells help B cells produce

IL-10, which in nonpathogenic conditions may inhibit inflammation against gut flora required for $V_\alpha19i$ T cell selection. Therefore, we propose a model of $V_\alpha19i$ T cell–induced protection from EAE whereby $V_\alpha19i$ T cells interact with B cells in lymphoid tissue through ICOS–B7RP-1 and to a lesser degree through other costimulatory pathways to induce IL-10 production, which in turn can inhibit the production of disease-promoting T_H1 cytokines such as IFN-γ and TNF. In conclusion, here we have identified a protective function for invariant $V_\alpha19i$ T cells in autoimmune disease. In contrast to 'conventional' $V_\alpha14i$ NKT cells, more T cells express the $V_\alpha19i$ TCR human homolog $V_\alpha7.2$-$J_\alpha33$ than in mice and therefore these cells may prove to be useful therapeutic targets for the treatment of autoimmune disease.

METHODS

Mice and induction of EAE. C57BL/6 mice (CLEA Laboratory Animal), μMT mice (Jackson Laboratories), $V_\alpha19iTg$ mice[5], $V_\alpha19iTgCd1d1^{-/-}$ mice, $Cd1d1^{-/-}$ mice and $Mr1^{-/-}$ mice[7] were maintained in specific pathogen–free conditions in accordance with institutional guidelines (National Institute of Neuroscience, Tokyo, Japan.). $Mr1^{-/-}$ mice were backcrossed to C57BL/6 mice for ten generations[24]. Mice were injected subcutaneously with 100 μg MOG(35–55) and 1 mg heat-killed *Mycobacterium tuberculosis* H37RA (Difco) emulsified in complete Freund's adjuvant. Pertussis toxin (200 ng in PBS; List Biological Laboratories) was injected intraperitoneally on days 0 and 2 after immunization. EAE clinical symptoms were assigned scores daily as follows: 0, no clinical signs; 1, loss of tail tonicity; 2, impaired righting reflex; 3, partial hindlimb paralysis; 4, total hindlimb paralysis.

Cell sorting and adoptive transfer. For depletion of NK cells, mice were injected intraperitoneally with 100 μg anti-asialo-GM_1 (ref. 44) 48 h before purification of $V_\alpha19i$ T cells. Liver or spleen cells were isolated from mice by Percoll density-gradient centrifugation, and NKT cells, B cells and T cells were purified with the AutoMACS cell purification system (Miltenyi Biotech). NKT cells were isolated using phycoerythrin-conjugated anti-NK1.1 (PK136; BD Pharmingen) and anti-phycoerythrin microbeads (Miltenyi Biotech). The purity of isolated $NK1.1^+$ T cells, assessed by flow cytometry, was more than 90%. In some experiments, single-cell suspensions were incubated with fluorescein isothiocyanate–anti-CD3 (2C11; BD Pharmingen) and phycoerythrin–anti-NK1.1 (PK136, BD Pharmingen) for sorting by flow cytometry. B cells and T cells were isolated from the spleen with anti-CD19 microbeads or the 'pan T cell' kit (Miltenyi Biotech). For adoptive transfer studies, liver $CD3^+NK1.1^+$ $V_\alpha19i$ T cells were sorted from naive $V_\alpha19iTgCd1d1^{-/-}$ mice as described above, and 1×10^6 $V_\alpha19i$ T cells were injected intraperitoneally into naive C57BL/6 recipient mice on the day of immunization with MOG(35–55). Control groups received identical numbers of $CD3^+NK1.1^-$ hepatic cells.

Cell proliferation and cytokine analysis. For *in vitro* stimulation of sorted $V_\alpha19i$ T cells, $CD3^+NK1.1^+$ and $CD3^+NK1.1^-$ cells were suspended in RPMI 1640 medium (Sigma) supplemented with 10% FCS, 2 mM L-glutamine, 100 U/ml of penicillin-streptomycin, 2 mM sodium pyruvate and 50 μM β-mercaptoethanol and were stimulated with immobilized anti-CD3 (5 μg/ml; BD Pharmingen). Cytokines were measured with inflammation cytometric bead assay kits (BD Biosciences) at 24, 48 and 72 h after stimulation with mouse T_H1-T_H2 cytokines. At 10 d after EAE induction without pertussis toxin, myelin-specific T cell responses were measured. Lymphocytes (1×10^6) were cultured with MOG(35–55) (1–100 μM for proliferation studies and 100 μM for cytokine analysis). Cytokines were measured with a cytometric bead assay kit (BD Biosciences) or an IL-17 enzyme-linked immunosorbent assay kit (BD Pharmingen) at 72 h after stimulation. Identical sets of wells were used for proliferation studies. After 72 h, cells were incubated with [^{3}H]thymidine (1 μCi/well) for the final 16 h of culture and incorporation of radioactivity was analyzed with a β-1205 counter (Pharmacia). Proliferation was determined from triplicate wells for each peptide concentration and is expressed as counts per minute.

Surface marker analysis, quantification of CNS leukocytes and histology. The surface phenotype of sorted $V_\alpha19i$ T cells was analyzed by flow cytometry. Nonspecific staining was inhibited by incubation with anti-CD16/32 (BD Pharmingen). Cells were then stained with fluorescence-labeled antibodies specific for CD4, NK1.1, TCRβ, CD3, CD44, CD49d, CD19, CD8, CD14, CD28, CD278, CD86 or CD154 (BD Pharmingen) or CCR1 and CCR2 (Santa Cruz), followed by phycoerythrin-conjugated anti–goat immunoglobulin G (Santa Cruz), and were analyzed with a FACSCalibur (Becton Dickinson). Intracellular cytokines were analyzed by flow cytometry with the BD Cytofix/Cytoperm kit (BD Pharmingen). Staining of paraffin-embedded spinal cords with luxol fast blue and with haematoxylin and eosin was done by SRL. For quantification by flow cytometry, spinal cords were homogenized through 70-μm nylon mesh and by Percoll density-gradient centrifugation to form single-cell suspensions.

RNA extraction and real-time RT-PCR. The SV Total RNA isolation kit (Promega) was used for isolation of total RNA from sorted liver or splenic NKT cells, T cells or B cells according to the manufacturer's instructions. First-strand cDNA was generated with the Advantage-RT kit (Clontech). The Light Cycler-FastStart DNA Master SYBR Green I kit (Roche Diagnostics) was used for real-time PCR. Gene expression values were normalized to expression of the hypoxanthine guanine phosphoribosyl transferase (*Hprt1*) 'housekeeping' gene. Primers from Bex Co are listed in **Supplementary Table 1** online.

Mixed-lymphocyte experiments. MOG(35–55)-specific spleen cells (2×10^6) isolated from wild-type nontransgenic mice 10 d after EAE induction were mixed with liver $V_\alpha19i$ T cells (5×10^5) sorted from naive $V_\alpha19iTgCd1d1^{-/-}$ mice, in the presence of 100 μg/ml of MOG(35–55) in 24-well plates or transwell plates (Corning). Where indicated, MOG(35–55)-specific spleen cells were isolated from $Mr1^{-/-}$ or μMT mice or were subjected to depletion with anti-CD19 microbeads (Miltenyi Biotech). Costimulatory molecules were blocked with 10 μg/ml of anti-B7RP-1 (HK5.3) or anti-CD40L (MR1) or with anti-CD80 and anti-CD86 (16-10A1 and GL1, respectively; all from BD Pharmingen)[35]. After 72 h, cytokines in the supernatant were analyzed by cytometric bead assay, enzyme-linked immunosorbent assay or intracellular flow cytometry. Proliferation of MOG(35–55)-specific lymph node cells was assessed 24 h after the addition of [^{3}H]thymidine (1 μCi/well) to 96-well plates.

Statistics. EAE clinical scores for groups of mice are presented as the mean group clinical score ± s.e.m., and statistical differences were analyzed by the Mann-Whitney U nonparametric ranking test. Cytokine secretion data were analyzed with the two-tailed Student's *t*-test or one-way analysis of variance with Tukey post-analysis for multiple group analysis.

Note: Supplementary information is available on the Nature Immunology website.

ACKNOWLEDGMENTS

We thank S. Gilfillan (Department of Pathology and Immunology, Washington University School of Medicine, St. Louis, Missouri) for $Mr1^{-/-}$ mice. Supported by the Japan Society for the Promotion of Science (P03581 to J.L.C), the Ministry of Health, Labour and Welfare of Japan (T.Y. and S.M.), The Program for Promotion of Fundamental Studies in Health Sciences of the National Institute of Biomedical Innovation (02-5 to T.Y.), Grant-in-Aid for Science Research on Priority Area from Ministry of Education, Science, Sports and Culture of Japan (17047051 to S.M.) and Grant-in-Aid for Scientific Research (B) (18390295 to S.M.) from the Japan Society for the Promotion of Science.

COMPETING INTERESTS STATEMENT

The authors declare that they have no competing financial interests.

Published online at http://www.nature.com/natureimmunology/
Reprints and permissions information is available online at http://npg.nature.com/reprintsandpermissions/

1. Kronenberg, M. Toward an understanding of NKT cell biology: progress and paradox. *Annu. Rev. Immunol.* **23**, 877–900 (2005).
2. Treiner, E. *et al.* Mucosal-associated invariant T (MAIT) cells: an evolutionarily conserved T cell subset. *Microbes Infect.* **7**, 552–559 (2005).
3. Kawano, T. *et al.* CD1d-restricted and TCR-mediated activation of Vα14 NKT cells by glycosylceramides. *Science* **278**, 1626–1629 (1997).

4. Zhou, D. *et al.* Lysosomal glycosphingolipid recognition by NKT cells. *Science* **306**, 1786–1789 (2004).
5. Okamoto, N. *et al.* Synthetic α-mannosyl ceramide as a potent stimulant for an NKT cell repertoire bearing the invariant $V_{\alpha}19$-$J_{\alpha}26$ TCR α chain. *Chem. Biol.* **12**, 677–683 (2005).
6. Chen, Y.H., Chiu, N.M., Mandal, M., Wang, N. & Wang, C.R. Impaired $NK1^+$ T cell development and early IL-4 production in CD1-deficient mice. *Immunity* **6**, 459–467 (1997).
7. Treiner, E. *et al.* Selection of evolutionarily conserved mucosal-associated invariant T cells by MR1. *Nature* **422**, 164–169 (2003).
8. Spada, F.M., Koezuka, Y. & Porcelli, S.A. CD1d-restricted recognition of synthetic glycolipid antigens by human natural killer T cells. *J. Exp. Med.* **188**, 1529–1534 (1998).
9. Tilloy, F. *et al.* An invariant T cell receptor α chain defines a novel TAP-independent major histocompatibility complex class Ib-restricted α/β T cell subpopulation in mammals. *J. Exp. Med.* **189**, 1907–1921 (1999).
10. Godfrey, D.I., MacDonald, H.R., Kronenberg, M., Smyth, M.J. & Van Kaer, L. NKT cells: what's in a name? *Nat. Rev. Immunol.* **4**, 231–237 (2004).
11. Lehuen, A. *et al.* Overexpression of natural killer T cells protects Vα14-Jα281 transgenic nonobese diabetic mice against diabetes. *J. Exp. Med.* **188**, 1831–1839 (1998).
12. Mars, L.T. *et al.* Vα14-Jα281 NKT cells naturally regulate experimental autoimmune encephalomyelitis in nonobese diabetic mice. *J. Immunol.* **168**, 6007–6011 (2002).
13. Wagner, M.J., Hussain, S., Mehan, M., Verdi, J.M. & Delovtch, T.L. A defect in lineage fate decision during fetal thymic invariant NKT cell development may regulate susceptibility to type 1 diabetes. *J. Immunol.* **174**, 6764–6771 (2005).
14. Pál, E. *et al.* Costimulation-dependent modulation of experimental autoimmune encephalomyelitis by ligand stimulation of Vα14 NK T cells. *J. Immunol.* **166**, 662–668 (2001).
15. Sharif, S. *et al.* Activation of natural killer T cells by α-galactosylceramide treatment prevents the onset and recurrence of autoimmune type 1 diabetes. *Nat. Med.* **7**, 1057–1062 (2001).
16. Hong, S. *et al.* The natural killer T-cell ligand α-galactosylceramide prevents autoimmune diabetes in non-obese diabetic mice. *Nat. Med.* **7**, 1052–1056 (2001).
17. Miyamoto, K., Miyake, S. & Yamamura, T. A synthetic glycolipid prevents autoimmune encephalomyelitis by inducing T_H2 bias of natural killer T cells. *Nature* **413**, 531–534 (2001).
18. Chiba, A. *et al.* Suppression of collagen-induced arthritis by natural killer T cell activation with OCH, a sphingosine-truncated analog of α-galactosylceramide. *Arthritis Rheum.* **50**, 305–313 (2004).
19. Miyake, S. & Yamamura, T. Therapeutic potential of glycolipid ligands for natural killer (NK) T cells in the suppression of autoimmune diseases. *Curr. Drug Targets Immune Endocr. Metabol. Disord.* **5**, 315–322 (2005).
20. Chiba, A., Kaieda, S., Oki, S., Yamamura, T. & Miyake, S. The involvement of Vα14 natural killer T cells in the pathogenesis of arthritis in murine models. *Arthritis Rheum.* **52**, 1941–1948 (2005).
21. Kim, H.Y. *et al.* NKT cells promote antibody-induced joint inflammation by suppressing transforming growth factor β1 production. *J. Exp. Med.* **201**, 41–47 (2005).
22. Porcelli, S., Yockey, C.E., Brenner, M.B. & Balk, S.P. Analysis of T cell antigen receptor (TCR) expression by human peripheral blood $CD4^-8^-$ α/β T cells demonstrates preferential use of several V_{β} genes and an invariant TCR α chain. *J. Exp. Med.* **178**, 1–16 (1993).
23. Shimamura, M. & Huang, Y.Y. Presence of a novel subset of NKT cells bearing an invariant Vα19.1-Jα26 TCR α chain. *FEBS Lett.* **516**, 97–100 (2002).
24. Kawachi, I., Maldonado, J., Strader, C. & Gilfillan, S. MR1-restricted Vα19i mucosal-associated invariant T cells are innate T cells in the gut lamina propria that provide a rapid and diverse cytokine response. *J. Immunol.* **176**, 1618–1627 (2006).
25. Illés, Z., Shimamura, M., Newcombe, J., Oka, N. & Yamamura, T. Accumulation of Vα7.2-Jα33 invariant T cells in human autoimmune inflammatory lesions in the nervous system. *Int. Immunol.* **16**, 223–230 (2004).
26. Illés, Z. *et al.* Differential expression of NK T cell Vα24JαQ invariant TCR chain in the lesions of multiple sclerosis and chronic inflammatory demyelinating polyneuropathy. *J. Immunol.* **164**, 4375–4381 (2000).
27. Croxford, J.L., Feldmann, M., Chernajovsky, Y. & Baker, D. Different therapeutic outcomes in experimental allergic encephalomyelitis dependent upon the mode of delivery of IL-10: a comparison of the effects of protein, adenoviral or retroviral IL-10 delivery into the central nervous system. *J. Immunol.* **166**, 4124–4130 (2001).
28. Croxford, J.L. *et al.* Cytokine gene therapy in experimental allergic encephalomyelitis by injection of plasmid DNA-cationic liposome complex into the central nervous system. *J. Immunol.* **160**, 5181–5187 (1998).
29. Cua, D.J., Groux, H., Hinton, D.R., Stohlman, S.A. & Coffman, R.L. Transgenic interleukin 10 prevents induction of experimental autoimmune encephalomyelitis. *J. Exp. Med.* **189**, 1005–1010 (1999).
30. Bettelli, E., Nicholson, L.B. & Kuchroo, V.K. IL-10, a key effector regulatory cytokine in experimental autoimmune encephalomyelitis. *J. Autoimmun.* **20**, 265–267 (2003).
31. Langrish, C.L. *et al.* IL-23 drives a pathogenic T cell population that induces autoimmune inflammation. *J. Exp. Med.* **201**, 233–240 (2005).
32. Fillatreau, S., Sweenie, C.H., McGeachy, M.J., Gray, D. & Anderton, S.M. B cells regulate autoimmunity by provision of IL-10. *Nat. Immunol.* **3**, 944–950 (2002).
33. Mauri, C., Gray, D., Mushtaq, N. & Londei, M. Prevention of arthritis by interleukin 10-producing B cells. *J. Exp. Med.* **197**, 489–501 (2003).
34. Riegert, P., Wanner, V. & Bahram, S. Genomics, isoforms, expression, and phylogeny of the MHC class I-related MR1 gene. *J. Immunol.* **161**, 4066–4077 (1998).
35. Hayakawa, Y. *et al.* Differential regulation of Th1 and Th2 functions of NKT cells by CD28 and CD40 costimulatory pathways. *J. Immunol.* **166**, 6012–6018 (2001).
36. Ikarashi, Y. *et al.* Dendritic cell maturation overrules H-2D-mediated natural killer T (NKT) cell inhibition: critical role for B7 in CD1d-dependent NKT cell interferon γ production. *J. Exp. Med.* **194**, 1179–1186 (2001).
37. Kitamura, H. *et al.* The natural killer T (NKT) cell ligand α-galactosylceramide demonstrates its immunopotentiating effect by inducing interleukin (IL)-12 production by dendritic cells and IL-12 receptor expression on NKT cells. *J. Exp. Med.* **189**, 1121–1128 (1999).
38. Kaneda, H. *et al.* ICOS costimulates invariant NKT cell activation. *Biochem. Biophys. Res. Commun.* **327**, 201–207 (2005).
39. Hutloff, A. *et al.* ICOS is an inducible T-cell co-stimulator structurally and functionally related to CD28. *Nature* **397**, 263–266 (1999).
40. McAdam, A.J. *et al.* ICOS is critical for CD40-mediated antibody class switching. *Nature* **409**, 102–105 (2001).
41. Song, F. *et al.* Expression of the neutrophil chemokine KC in the colon of mice with enterocolitis and by intestinal epithelial cell lines: effects of flora and proinflammatory cytokines. *J. Immunol.* **162**, 2275–2280 (1999).
42. Kaneko, M., Akiyama, Y., Takimoto, H. & Kumazawa, Y. Mechanism of up-regulation of immunoglobulin A production in the intestine of mice unresponsive to lipopolysaccharide. *Immunology* **116**, 64–70 (2005).
43. Cognasse, F. *et al.* Differential downstream effects of CD40 ligation mediated by membrane or soluble CD40L and agonistic Ab: a study on purified human B cells. *Int. J. Immunopathol. Pharmacol.* **18**, 65–74 (2005).
44. Muhlen, K.A. *et al.* NK cells, but not NKT cells, are involved in *Pseudomonas aeruginosa* exotoxin A-induced hepatotoxicity in mice. *J. Immunol.* **172**, 3034–3041 (2004).

Brain Advance Access published July 10, 2006

doi:10.1093/brain/awl170 *Brain* (2006) Page 1 of 9

Selective COX-2 inhibitor celecoxib prevents experimental autoimmune encephalomyelitis through COX-2-independent pathway

Katsuichi Miyamoto,[1,2] Sachiko Miyake,[1] Miho Mizuno,[1] Nobuyuki Oka,[3] Susumu Kusunoki[2] and Takashi Yamamura[1]

[1]Department of Immunology, National Institute of Neuroscience, NCNP, Tokyo, [2]Department of Neurology, Kinki University School of Medicine, Osaka and [3]Department of Rehabilitation Medicine, Minami-kyoto National Hospital, Kyoto, Japan

Correspondence to: Sachiko Miyake, Department of Immunology, National Institute of Neuroscience, NCNP, Kodaira, Tokyo 187-8502, Japan
E-mail: miyake@ncnp.go.jp

Cyclooxygenase (COX) is a key enzyme of arachidonic acid metabolism and exists as two distinct isoforms. COX-1 is constitutively expressed in most tissues, whereas COX-2 is inducibly expressed at the site of inflammation. Selective inhibitors of COX-2 have been developed and have been used as anti-inflammatory agents. Here, we show that a new-generation COX-2 inhibitor, celecoxib, inhibited experimental autoimmune encephalomyelitis (EAE). Celecoxib, but not other COX-2 inhibitors such as nimesulid, prevented myelin oligodendrocyte glycoprotein (MOG) induced EAE when administrated orally on the day of disease induction. Moreover, celecoxib inhibited EAE in COX-2-deficient mice, indicating that celecoxib inhibited EAE in a COX-2-independent manner. In celecoxib-treated mice, interferon-γ (IFN-γ) production from MOG-specific T cells was reduced and MOG-specific IgG1 was elevated compared with vehicle-treated mice. Infiltration of inflammatory cells into the central nervous system and the expression of adhesion molecules, P-selectin and intercellular adhesion molecule-1 (ICAM-1), and a chemokine, monocyte chemoattractant peptide-1 (MCP-1), were inhibited when mice were treated with celecoxib. These results suggest that celecoxib may be useful as a new additional therapeutic agent for multiple sclerosis.

Keywords: COX-2 inhibitor; celecoxib; experimental autoimmune encephalomyelitis; multiple sclerosis

Abbreviations: CMC = carboxymethylcellulose; COX = cyclooxygenase; EAN = experimental autoimmune neuritis; EAE = experimental autoimmune encephalomyelitis; ELISA = enzyme-linked immunosorbent assay; ICAM-1 = intercellular adhesion molecule-1; IFN = interferon; IL = interleukin; LN = lymph node; MCP-1 = monocyte chemoattractant peptide-1; MOG = myelin oligodendrocyte glycoprotein; PBS = phosphate-buffered saline

Received February 6, 2006. Revised April 11, 2006. Accepted May 31, 2006

Introduction

Cyclooxygenase (COX) catalyses the conversion of arachidonic acid to prostaglandins and has two isoforms, COX-1 and COX-2 (Vane *et al.*, 1994; Warner and Mitchell, 2004). COX-1 is constitutively expressed in most tissues and produces prostaglandins involved in maintenance of the gastric mucosa, regulation of renal blood flow and platelet aggregation. On the other hand, COX-2 is inducibly expressed in cells involved in inflammation and in neoplastic tissues by proinflammatory and mitogenic stimuli, and is primarily responsible for the synthesis of prostanoids involved in acute and chronic inflammation (Xie *et al.*, 1997). COX-2 therefore appears to be a suitable target for the anti-inflammatory effects of non-steroidal anti inflammatory drugs. These findings have provided the rationale for the development of selective inhibitors of COX-2.

Celecoxib is a new generation of highly specific COX-2 inhibitors that have been approved for the treatment of rheumatoid arthritis and other inflammatory diseases. The selectivity of COX-2 inhibition is much higher than traditional COX-2 inhibitors (Penning *et al.*, 1997). Furthermore, celecoxib has been shown to exert a potent anti-tumour effect. Interestingly, the anti-tumour effect by celecoxib

has been reported via both COX-2-dependent and COX-2-independent mechanisms (Grosch *et al.*, 2001). For example, cell cycle arrest and apoptosis of various kinds of cells induced by celecoxib appeared to be COX-2-independent effects (Hsu *et al.*, 2000; Arico *et al.*, 2002; Liu *et al.*, 2004).

Experimental autoimmune encephalomyelitis (EAE) is a widely used animal model for multiple sclerosis that can be induced by immunization with myelin antigens such as myelin oligodendrocyte glycoprotein (MOG). EAE is mediated primarily by $CD4^+$ Th1 T cells producing interferon-γ (IFN-γ) and tumour necrosis factor-α (TNF-α) (Nicholson and Kuchroo, 1996; Kumar *et al.*, 1997; Zhang *et al.*, 1997). COX-2 is expressed in neurons and endothelial cells in healthy brain. In rats with EAE, the expression of COX-2 was reported to be upregulated in endothelial cells in inflammatory lesions. In addition, non-selective COX-2 inhibitors have been reported to moderately ameliorate EAE (Prosiegel *et al.*, 1989; Weber *et al.*, 1991; Simmons *et al.*, 1992), suggesting that COX-2 may have an important role in the pathogenesis of EAE (Deininger and Schluesener, 1999). Furthermore, we recently demonstrated that COX-2 inhibitors suppress experimental autoimmune neuritis (EAN), a model of Guillain–Barré syndrome, which is also characterized as a $CD4^+$-Th1 T-cell-mediated autoimmune neurological disease model similar to EAE (Miyamoto *et al.*, 1998, 1999, 2002). These findings led us to investigate the effect of COX-2 inhibitors on EAE.

In the present study, we found that celecoxib greatly suppressed EAE in comparison with traditional COX-2 inhibitors. Furthermore, we have demonstrated that celecoxib inhibited EAE by inhibiting Th1 response of autoreactive T cells and that this inhibition was COX-2-independent. Finally, we demonstrated that celecoxib prevented cell entry into the CNS in association with the inhibition of the expression of P-selectin, intercellular adhesion molecule-1 (ICAM-1) and monocyte chemoattractant peptide-1 (MCP-1). These results highlighted the COX-2-independent therapeutic potential of celecoxib for multiple sclerosis.

Material and methods

Mouse

Wild-type C57BL/6 (B6) mice were purchased from Clea Japan (Tokyo, Japan). COX-2-deficient mice ($COX\text{-}2^{-/-}$) have been backcrossed to B6 background for more than five generations and were purchased from Taconic (Germantown, NY, USA). These mice were maintained under specific pathogen-free conditions.

Induction of EAE

For induction of EAE, mice were immunized (5–10 mice per group) subcutaneously in flanks with 100 μg of $MOG_{35–55}$ peptide (MEVGWYRSPFSRVVHLYRNGK) in 0.1 ml phosphate-buffered saline (PBS) and 0.1 ml complete Freund's adjuvant (CFA) containing 1 mg *Mycobacterium tuberculosis* H37Ra (Difco Laboratories, Detroit, MI, USA) and were injected intravenously with 200 ng of pertussis toxin (List Biological Laboratories, Campbell, CA, USA) on the day of immunization and 2 days later.

Clinical assessment of EAE

EAE was scored on the following scale: 0 = no clinical signs; 1 = partial loss of tail tonicity; 2 = completely limp tail and abnormal gait; 3 = partial hindlimb paralysis; 4 = complete hindlimb paralysis; and 5 = fore- and hindlimb paralysis or moribund state.

Treatment with COX-2 inhibitors

Mice were orally administered 5 μg/g of COX-2 inhibitor, celecoxib (Searle, St Louis, MO, USA) (Penning *et al.*, 1997), nimesulid (Nakarai Tesque, Kyoto, Japan) (Nakatsuji *et al.*, 1996), or indomethacin (Nakarai Tesque) in 0.5% carboxymethylcellulose (CMC) via a feeding cannula every 2 days. Control mice were orally administered vehicle (0.5% CMC) alone.

Measurement of $MOG_{35–55}$-specific IgG1 and IgG2a titres

Enzyme-linked immunosorbent assay (ELISA) plates (Sumitomo, Tokyo, Japan) were coated with 10 μg/ml $MOG_{35–55}$ in PBS overnight at 4°C. After blocking with 2% bovine serum albumin (BSA) in PBS, different dilutions of the serum from animals at Day 30 after immunization, or normal mice or PBS were added to the plate. $MOG_{35–55}$-specific antibodies were detected using biotin-labelled anti-IgG1 and anti-IgG2a antibodies (Vector Laboratories, Burlingame, CA, USA). After adding streptavidin-peroxidase (BD Biosciences, San Jose, CA, USA) and a substrate, plates were read at OD_{450} values.

$MOG_{35–55}$-specific T-cell proliferation assay

On Day 11 after immunization with $MOG_{35–55}$, draining lymph nodes (LN) were harvested and single cell suspensions were prepared. Cells were cultured in RPMI1640 medium (Gibco, Grand Island, NY, USA) supplemented with 5×10^{-5} M 2-mercaptoethanol, 2 mM L-glutamine, 100 U/ml penicillin and streptomycin and 1% autologous mouse serum, and seeded onto 96-well flat-bottom plates (1×10^6 cells/well). The cells were stimulated with peptide for 72 h at 37°C in a humidified air condition with 5% CO_2. To measure cellular proliferation, [^{3}H]-thymidine was added (1 μCi/well) and uptake of the radioisotope during the final 18 h of culture was counted with a beta-1205 counter (Pharmacia, Uppsala, Sweden). To evaluate proliferative responses of LN cells to peptide, we determined the Δc.p.m. value for cells in each well by subtracting the background c.p.m.

Detection of cytokines and chemokine

LN cells from the $MOG_{35–55}$-immunized mice were cultured in the standard medium in 96-well flat-bottom plates at 1×10^6/well for 48 h in the presence of the different concentrations of $MOG_{35–55}$. The concentrations of IFN-γ, interleukin-4 (IL-4) and IL-10 in the supernatants were measured by using a sandwich ELISA following the protocol provided by BD Biosciences. A chemokine, MCP-1, in the serum from mice on Day 7, 10 and 14 after induction of EAE was also measured by using a sandwich ELISA following the protocol provided by BD Biosciences. All reagents, including recombinant mouse cytokines, chemokine and antibodies were purchased from BD Biosciences.

Analysis of infiltrating cells isolated from CNS

Mice were anaesthetized with diethyl ether on Day 14 after induction of EAE. After perfusion with PBS, brain and spinal cord were removed and homogenized. After washing with PBS, mononuclear cells were isolated using Ficoll gradient (Amersham Biosciences, Piscataway, NJ, USA) (Krakowski *et al.*, 1997). The cells were stained with APC-labelled anti-CD3 antibody, fluoroisothiocyanate (FITC) labelled anti-CD4 or CD8 or CD19 antibody (BD Biosciences) and were analysed by flow cytometer (BD FACS Calibur). Apoptosis of lymphocytes was analysed by using Annexin-5 apoptosis kit (BD Biosciences).

Pathological analysis

The brain and spinal cord were removed on Day 7, 10 and 14 after induction of EAE. Ten-micrometre frozen sections were fixed with acetone and stained with haematoxylin and eosin (HE), Luxol fast blue or antibodies of adhesion molecule ICAM-1 (CD54), vascular cell adhesion molecule-1 (VCAM-1: CD106), E-selectin (CD62E) and P-selectin (CD62P) (BD Biosciences), following the protocol provided by BD Biosciences.

Statistics

For statistic analysis, non-parametric Mann–Whitney *U*-test was used to calculate significant levels for all measurements. Values of $P < 0.05$ were considered statistically significant.

Results

Celecoxib inhibits EAE

To examine the effect of celecoxib on the development of EAE, we first administered celecoxib at the time of immunization with MOG_{35-55}. Oral administration of celecoxib reduced the incidence of disease and suppressed maximum EAE score and cumulative score compared with the control group (Fig. 1A, Table 1). Histological comparison between the thoracic region of the spinal cord demonstrated reduced monocyte infiltration and demyelination in cerecoxib-treated mice compared with vehicle-treated mice (Fig. 2A–D). Celecoxib was also effective in reducing the severity of disease when administered at Day 8

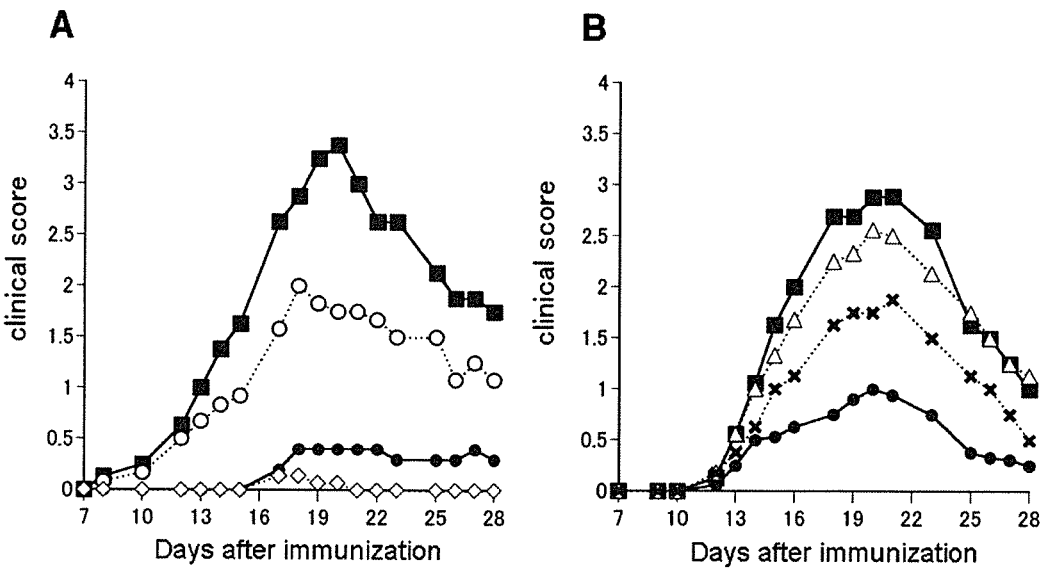

Fig. 1 Effect of celecoxib on actively induced EAE. EAE was induced in female B6 mice by immunization with MOG_{35-55} in CFA as described in Material and methods. (**A**) Mice were orally administered 5 μg/g (closed circles) or 10 μg/g (open diamond) of celecoxib starting from the day of the immunization, or with 5 μg/g of celecoxib starting from 8 days after the immunization (open circles). Control mice were administered vehicle alone (closed squares). Statistical analysis is shown in Table 1. (**B**) Mice were orally administered 5 μg/g of celecoxib (closed circles) or nimesulid (open triangle) or indomethacin (crosses) every 2 days from the day of EAE induction. Control mice were administered vehicle alone (closed squares). Statistical analysis is shown in Table 2. One representative experiment of two independent experiments is expressed as mean ± SEM.

Table 1 Clinical scores of EAE treated with celecoxib

	Max. score	Day of onset	Incidence (%)	Cumulative score
Control (CMC)	3.50 ± 0.20	12.50 ± 1.56	100 (10/10)	33.00 ± 5.05
Celecoxib 10 μg/g	0.14 ± 0.05*	17.50 ± 0.50	20.0 (2/10)	0.42 ± 0.04*
Celecoxib 5 μg/g	0.40 ± 0.40*	17.00 ± 0.00	20.0 (2/10)	3.80 ± 3.80*
Celecoxib 5 μg/g (from Day 8)	2.42 ± 0.57	14.20 ± 1.83	83.3 (10/12)	20.17 ± 5.22

Four groups of mice were immunized with MOG_{35-55} peptide for induction of EAE. The control CMC solution, 5 or 10 μg/g of celecoxib diluted in CMC, was orally injected via a cannula every 2 days starting from Day 0 or 8 after induction of EAE. Mean ± SEM of the following parameters are shown: maximum score of EAE (Max. score), the days of EAE onset, incidence of paralysed mice among sensitized mice (Incidence) and summation of the clinical scores from Day 0 to 30 (Cumulative score). *$P < 0.05$ versus control.

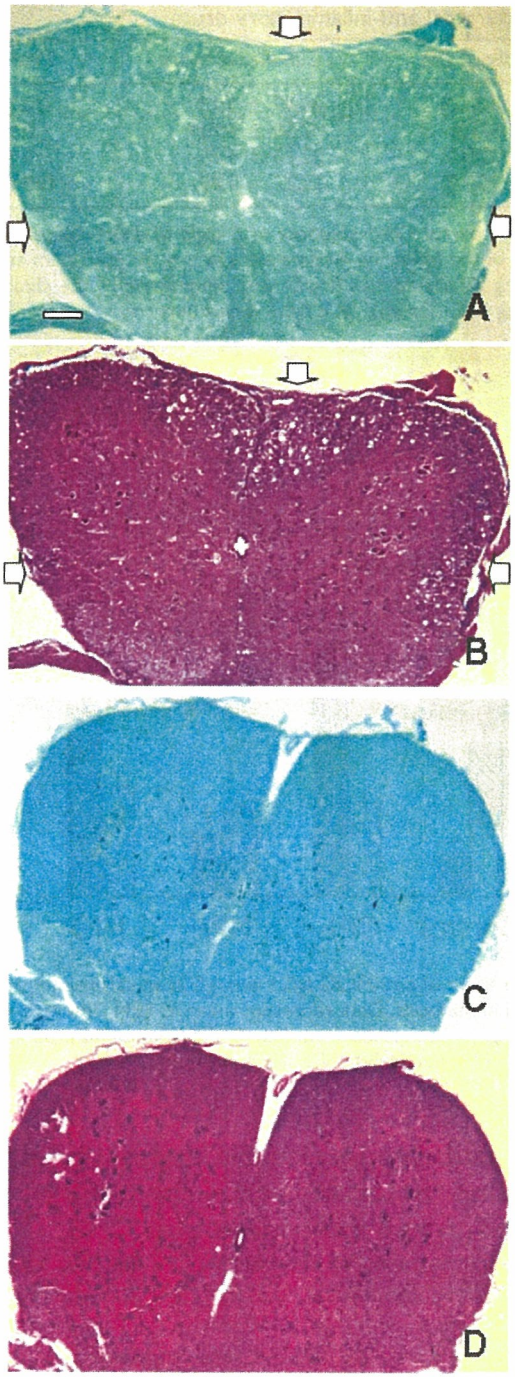

Fig. 2 Histopathological assessment of the CNS region in EAE-induced mice. Brains and spinal cords from EAE mice were removed on Day 14 after immunization as described in Material and methods. Thinly sliced (10 μm) frozen sections of the brains obtained from vehicle-treated mice (**A** and **B**) or celecoxib-treated mice (**C** and **D**) were stained with haematoxylin and eosin (**B** and **D**), or Luxol fast blue (**A** and **C**).

post-EAE-induction. Although indomethacin suppressed EAE to some extent, all mice died around Day 30 after immunization owing to intestinal ulcer. In contrast, oral administration of nimesulid, another COX-2 inhibitor, did not suppress either the incidence or the severity of EAE (Fig. 1B). Composite data from experiments is shown in Tables 1 and 2.

Celecoxib inhibits MOG-specific Th1 response

To determine the mechanisms by which celecoxib inhibits EAE, we examined the level of MOG-specific IgG1 and IgG2a in the serum samples collected from individual EAE-induced mice on Day 30. It is generally accepted that elevation of antigen-specific IgG2a antibody results from augmentation of a Th1 immune response to the antigen, whereas a higher level of IgG1 antibody would reflect a stronger Th2 response to the antigen. There was a significant elevation of the level of MOG_{35-55}-specific IgG1 and a slight reduction in the level of MOG-specific IgG2a in celecoxib-treated group compared with vehicle-treated group (Fig. 3A). In contrast, there was no significant difference in the level of either IgG1 or IgG2a in nimesulid-treated mice compared with vehicle-treated group (Fig. 3B).

To further investigate the response of T cells to MOG_{35-55} in celecoxib-treated mice, we examined the proliferative response and cytokine production of draining LN cells *in vitro*. Mice were immunized with MOG_{35-55} and were administered celecoxib or vehicle on the day of immunization. Ten days after immunization, draining LN cells were collected and cultured with MOG_{35-55} peptide. As shown in Fig. 4A, there was no significant difference in a proliferative response of MOG-reactive T cells between celecoxib-treated and vehicle-treated groups. We next examined the levels of cytokines in the culture supernatant by ELISA. The level of IFN-γ was reduced in the culture supernatants of LN cells obtained from mice treated with celecoxib compared with that from control mice (Fig. 4B). IL-4 and IL-10 were not detected in either culture supernatant. These results indicate that celecoxib reduces Th1 cytokine production from MOG-reactive T cells.

Celecoxib prevents EAE even in COX-2-deficient mice

Since another COX-2 inhibitor, nimesulid, did not have the inhibitory effect on EAE, we examined whether celecoxib could inhibit EAE in COX-2-deficient mice. As shown in Fig. 5A, the maximum EAE score, the day of onset and the severity of EAE were not significantly different between COX-$2^{-/-}$ and wild-type mice. Administration of celecoxib prevented the development of EAE in COX-$2^{-/-}$ mice as well as in wild-type mice. Consistent with the severity of EAE, the levels of MOG-specific IgG1 and IgG2a in COX-$2^{-/-}$ mice were not different compared with wild-type B6 mice (Fig. 5B). Moreover, celecoxib treatment increased the level of MOG-specific IgG1 even in COX-$2^{-/-}$ mice, resulting in the elevation of IgG1 : IgG2a ratio similar to that in wild-type mice (CMC = 0.29, celecoxib = 3.00) and COX-$2^{-/-}$ mice (CMC = 0.42, celecoxib = 2.52). These results indicate that the effect on the inhibition of EAE

Table 2 Clinical scores of EAE treated with celecoxib or other non-steroidal anti-inflammatory drugs

	Max. score	Day of onset	Incidence (%)	Cumulative score	Death (%)
Control (CMC)	3.05 ± 0.20	13.10 ± 1.16	100 (10/10)	26.47 ± 5.13	10 (1/10)
Celecoxib	1.02 ± 0.53*	14.30 ± 1.77	90 (9/10)	7.58 ± 6.72*	0 (0/10)
Nimesulid	2.54 ± 0.68	13.50 ± 1.56	100 (10/10)	22.15 ± 4.75	0 (0/10)
Indomethacin	1.70 ± 0.83	13.90 ± 1.93	100 (10/10)	15.21 ± 3.89	100 (10/10)*

Each mouse was immunized with MOG_{35-55} peptide for induction of EAE. The control CMC solution, or 5 μg/g of drugs diluted in CMC, was orally administered via a cannula every other day. Mean ± SEM of the following parameters are shown: maximum score of EAE (Max. score), the days of EAE onset, incidence of paralysed mice among sensitized rats (Incidence), summation of the clinical scores from Day 0 to 30 (Cumulative score) and the incidence of death during EAE (Death). *$P < 0.05$ versus control.

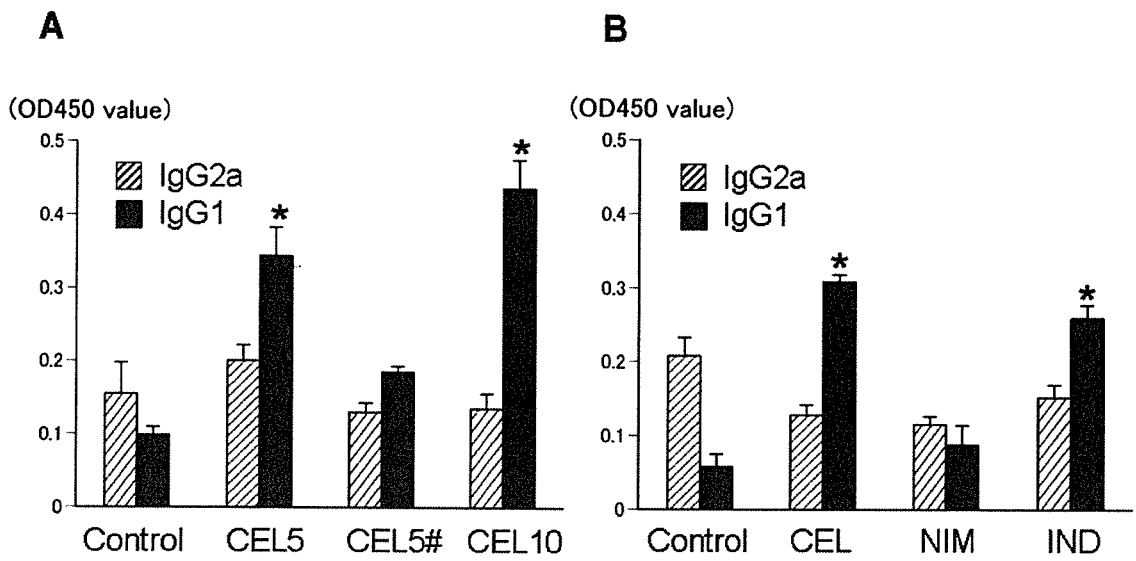

Fig. 3 Analysis of MOG_{35-55} IgG1 and IgG2a in EAE-induced mice. The relative titers of anti-MOG IgG1 and IgG2a in serum samples from individual mice ($n = 10$) on Day 30 after immunization were analysed as indicated in Methods. Data represent mean ± SEM. *$P < 0.05$ versus control. (**a**) Control = vehicle alone, CEL5 = 5 μg/g of celecoxib, CEL5# = 5 μg/g of celecoxib from Day 8 after the immunization, CEL10 = 10 μg/g of celecoxib. (**b**) Control = vehicle alone, CEL = celecoxib, NIM = nimesulid, IND = indomethacin.

and Th1 response by celecoxib is mediated by a COX-2-independent pathway (Table 3)

Celecoxib inhibits an infiltration of immune cells into CNS

To characterize the infiltrated cells into CNS, we isolated mononuclear cells from CNS obtained from celecoxib-treated or vehicle-treated mice. Mononuclear cells isolated from the CNS of vehicle-treated mice include $CD3^+$ T cells that comprised >80% of $CD4^+$ cells. In mice treated with celecoxib, the number of infiltrated cells was less than one-seventh compared with vehicle-treated mice (Table 4). In addition, we analysed apoptotic cells from CNS, spleen and draining LNs using annexin-5 staining. There was no difference in the frequency of apoptotic cells in all organs examined from celecoxib-treated and vehicle-treated mice (data not shown). These results suggest that celecoxib inhibits an infiltration of inflammatory cells into the CNS rather than induction of apoptosis of autoreactive T cells.

Celecoxib suppresses the expression of adhesion molecules and a chemokine related to cell infiltration into CNS

For the recruitment of autoreactive T cells into the brain through the blood–brain barrier (BBB), some adhesion molecules such as ICAM-1, VCAM-1 and P-selectin, and chemokines such as MCP-1 are required (Engelhardt *et al.*, 1997; Hofmann *et al.*, 2002). We performed an immunohistostaining of sliced brain sections from mice with EAE using antibodies against adhesion molecules. ICAM-1, VCAM-1 and P-selectin (Fig. 6A, C and E) were expressed on choroid plexus in the brain obtained from EAE-induced mice. In contrast, in brains obtained from celecoxib-treated mice, the expression level of P-selectin and ICAM-1 was lower compared with the control (Fig. 6B, D and F). In addition, we examined the level of MCP-1, which is an important chemokine involved in recruiting autoreactive T cells into the brain. As shown in Table 5, the level of MCP-1 in the serum obtained from

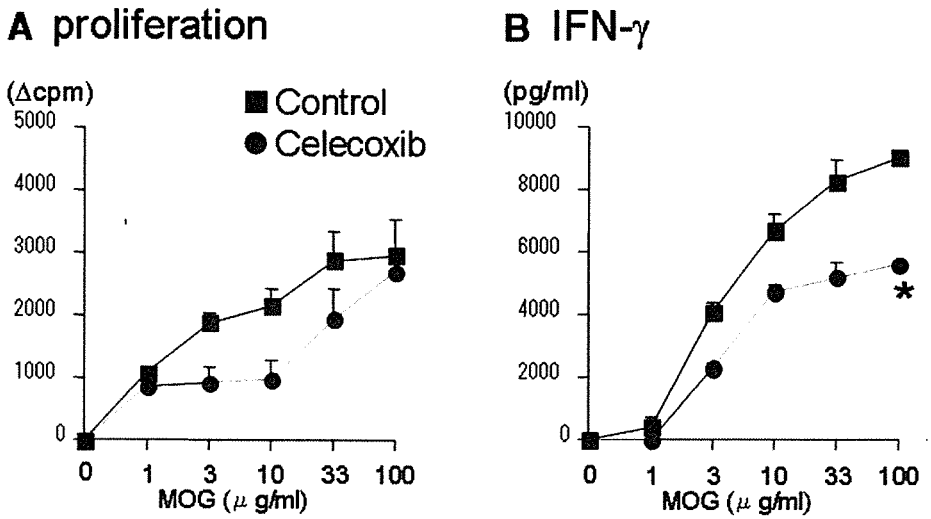

Fig. 4 Comparison of MOG_{35-55}-specific T-cell response after treatment with celecoxib. Popliteal and inguinal LN cells from treated and control animals were incubated in the presence of MOG_{35-55} for 48 h. Proliferative response was determined by the uptake of [^{3}H] thymidine (**A**), and IFN-γ was detected by ELISA (**B**). Representative data of two independent experiments are shown (n = 5 for each group). Error bars represent SEM. *P < 0.05 versus control.

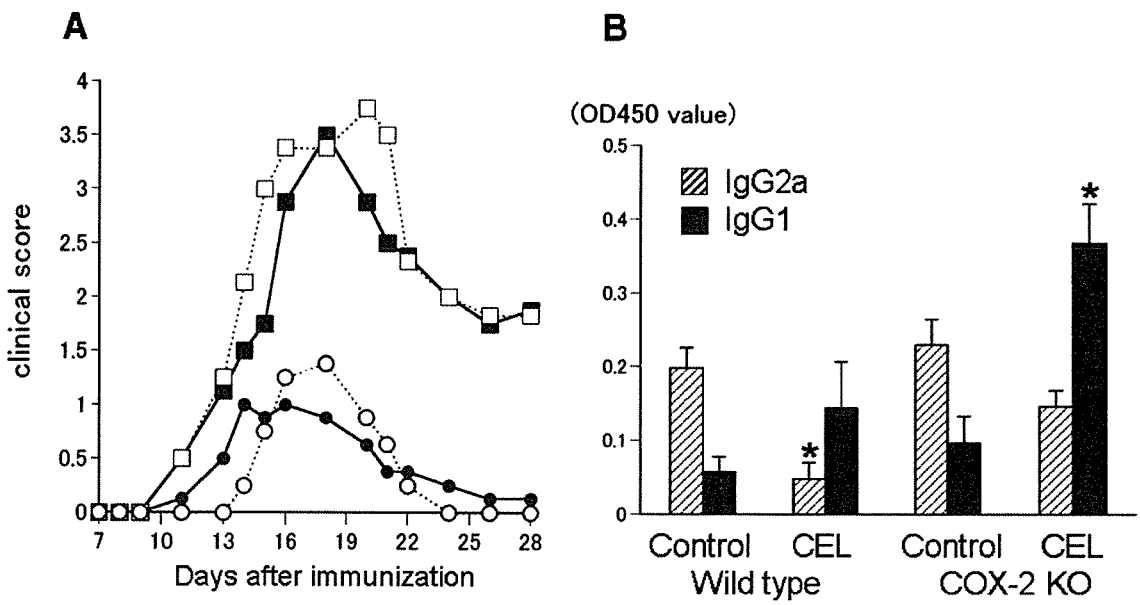

Fig. 5 Effect of celecoxib on actively induced EAE in COX-2-deficient mice. B6 mice and COX-2-deficient mice were immunized with MOG_{35-55} in CFA as described in Material and methods. (**A**) Mice were orally administered celecoxib (5 μg/g) every 2 days starting from the day of the immunization. Statistical analysis is shown in Table 3. Closed squares = vehicle alone for wild-type mice; closed circles = 5 μg/g of celecoxib for wild-type mice, open squares = vehicle alone for COX-2-deficient mice, open circles = 5 μg/g of celecoxib for COX-2-deficient mice. (**B**) The relative titres of anti-MOG IgG1 and IgG2a in serum samples from individual mice on Day 30 after immunization were analysed as indicated in Material and methods. Data represent mean ± SEM. *P < 0.05 versus control. Control = vehicle alone, CEL = celecoxib. One representative experiment of two independent experiments is expressed as mean ± SEM.

celecoxib-treated mice was significantly lower compared with that obtained from vehicle-treated mice. These findings suggested that celecoxib inhibits an infiltration of immune-mediated cells into CNS through the BBB by suppression of P-selectin, ICAM-1 and MCP-1.

Discussion

In the present study, we have demonstrated that a new-generation selective COX-2 inhibitor, celecoxib, strongly inhibited the development of EAE as compared with vehicle treatment or a traditional COX-2 inhibitor, nimesulid. The

Table 3 Clinical scores of EAE in COX-2-deficient mice

Mouse	Treatment	Max. score	Day of onset	Incidence (%)	Cumulative score
Wild-type	CMC	3.54 ± 0.28	12.60 ± 1.15	100 (10/10)	24.85 ± 6.37
	Celecoxib	1.13 ± 0.39*	13.20 ± 1.80	80 (8/10)	6.29 ± 4.02*
COX-2$^{-/-}$	CMC	3.75 ± 0.44	12.78 ± 1.57	100 (8/8)	29.88 ± 5.62
	Celecoxib	1.46 ± 0.51*	14.13 ± 1.96	87.5 (7/8)	5.39 ± 3.36*

Wild-type and COX-2$^{-/-}$ mice were immunized with MOG_{35-55} peptide to induce EAE. The control CMC solution, or 5 μg/g of celecoxib diluted in CMC, was administered every other day. Mean ± SEM of the following parameters are shown: maximum score of EAE (Max. score), the days of EAE onset, incidence of paralysed mice among sensitized mice (Incidence) and summation of the clinical scores from Day 0 to 30 (Cumulative score). *$P < 0.05$ versus control.

Table 4 Cell infiltration into the CNS of EAE-induced mice

	Mononuclear cell	$CD3^+$ cell	$CD4^+$ cell	$CD19^+$ cell
EAE mice				
Control (CMC)	667 ± 176	203 ± 69	158 ± 50	6 ± 1
Celecoxib	90 ± 57*	12 ± 8*	9 ± 5*	0 ± 0
Naive mice	20 ± 6	5 ± 2	3 ± 2	1 ± 0

CNS tissues from each group mouse were homogenized on Day 18 after immunization with MOG_{35-55} peptide. Mononuclear cells were isolated by Percoll solution. The cells were stained with cell markers and analysed by flow cytometer. Mean ± SEM of cell number (10^3 cells/mouse) is shown. Representative data of two independent experiments are shown ($n = 5$ for each group). *$P < 0.05$ versus control.

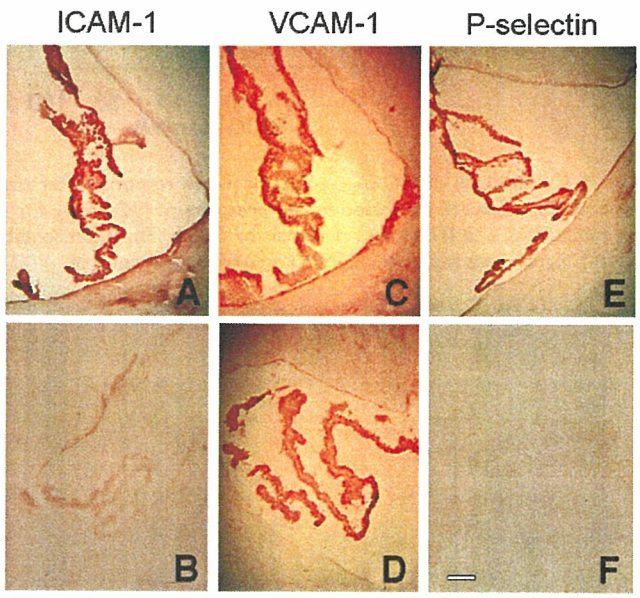

Fig. 6 Immunohistochemical staining with ICAM-1, VCAM-1 and P-selectin of the brain in EAE-induced mice. Brains from EAE mice were removed on Day 14 after immunization as described in Material and methods. Thinly sliced (10 μm) frozen sections of the brain were immunostained with anti-ICAM-1 antibody (**A** and **B**), anti-VCAM-1 antibody (**C** and **D**) and anti-P-selectin antibody (**E** and **F**). Figure shows choroid plexus region. Bar = 100 μm.

inhibitory effect on EAE by celecoxib was also evident in COX-2-deficient mice, indicating that celexoxib suppressed EAE in a COX-2-independent mechanism. In celecoxib-treated mice, MOG-specific Th1 responses were reduced and infiltration of immune cells was significantly inhibited compared with vehicle-treated mice, which were associated with lower expression of ICAM-1 and P-selectin on the choroid plexus in the brain.

Since EAE is an autoimmune inflammatory disease, administering COX-2 inhibitor was expected to inhibit disease as well as other COX inhibitors. Recently, Muthian *et al.* (2006) showed that some COX-2 inhibitors such as NS398 and LM01 suppressed EAE, when administered intraperitoneally every other day. In our study, we could not observe the inhibitory effect of nimesulid on EAE when orally administered every 2 days using the same conditions in which celecoxib exhibited a strong inhibitory effect. The route and timing of administration might be critical to modulate diseases. The inhibitory effect mediated by celecoxib was stronger compared with other COX inhibitors, suggesting that different mechanisms may be occurring in addition to the suppression of production of prostanoids that occurred at sites of disease and inflammation. In fact, COX-2 was not required for the celecoxib-mediated inhibitory effect on EAE. Recent studies have suggested that COX-2-independent pathways may contribute to celecoxib-mediated anti-tumour or anti-arthritic effect through enhanced apoptosis of tumour cells or synovial cells (Kusunoki *et al.*, 2002; Shishodia *et al.*, 2004). In our study, enhancing apoptosis of immune cells was not detected, indicating that different COX-2-independent mechanisms might be important for celecoxib-mediated inhibition of EAE. We observed that celecoxib treatment inhibited Th1 responses of MOG-reactive T cells. In the regulation of Th1/Th2 responses, prostaglandin E2 synthesized by COX has been reported to suppress IL-2 and IFN-γ production by a Th1 clone (Snijdewint *et al.*, 1993). In addition, Meyer *et al.* (2003) reported that administration of COX-2 inhibitor, NS398, increased *Helicobacter*-stimulated IL-12 and IFN-γ production, suggesting that COX-2 inhibition resulted in enhanced Th1 responses. In contrast, celecoxib inhibited Th1 responses of autoreactive T cells. Therefore, this COX-2-independent effect on immune system may be a mechanism to explain why celecoxib suppresses EAE to a greater degree compared with that of other COX-2 inhibitors. Allonza *et al.* (2006) reported that

Table 5 Serum level of MCP-1 in EAE mice after treatment with celecoxib

	Day 0	Day 7	Day 10	Day 14
EAE mice				
Control (CMC) (n = 18)	ND	60.0 ± 21.0	42.6 ±17.0	ND
Celecoxib (n = 16)	ND	8.5 ± 5.0*	12.9 ± 8.5	ND
Naive mice (n = 10)	ND	ND	ND	ND

B6 mice were immunized with MOG_{35-55} peptide as described in Material and methods. Serum samples from individual mice were collected on Day 0, 7, 10 and 14 after immunization. Serum concentration of MCP-1 was measured by ELISA. Data represent mean ± SEM (pg/ml). ND = not detectable. *$P < 0.05$ versus control.

celecoxib inhibits IL-12 αβ and β2 folding and secretion in association with the increased interaction of IL-12 with calreticulin, an endoplasmic reticulum-resident chaperone in retention of misfolded cargo proteins, while blocking interaction with Erp44. They also demonstrated that an analogue of celecoxib lacking the COX-2 inhibitor activity showed identical effects to that of celecoxib on folding and secretion of IL-12, indicating that the effect is COX-2-independent. Since IL-12 is a key cytokine to provoke Th1 immune response, reduction in MOG-specific Th1 response is consistent with these previous findings.

The infiltration of immune cells in the CNS was significantly inhibited in celecoxib-treated mice. Celecoxib has been reported to reduce expression of P-selectin and ICAM-1 in experimental inflammatory models such as experimental colitis (Cuzzocrea *et al.*, 2001, 2002). In our study, we observed that celecoxib suppressed expression of P-selectin and ICAM-1 in the brain of EAE mice. Since P-selectin and ICAM-1 are the adhesion molecules involved in the recruitment of inflammatory cells into CNS (Engelhardt *et al.*, 1997; Dietrich, 2002; Scott *et al.*, 2004), inhibition of cellular infiltration by celecoxib might be mediated by the downregulation of the expression of adhesion molecules.

Chemokines are also required for recruitment of immune cells into the CNS. MCP-1 is reported to be an essential chemokine in EAE (Hofmann *et al.*, 2002). In the mouse model of atherosclerosis, Wang *et al.* (2005) reported that celecoxib decreased the inflammatory response and hyperplasia following vascular injury through inhibition of MCP-1 induction. We detected a decreased level of MCP-1 in the serum in celecoxib-treated mice on EAE. The suppression of MCP-1 by celecoxib might also contribute to the reduction of infiltrating cells into the CNS.

In conclusion, celecoxib has a potent therapeutic potential for EAE by inducing a Th2 bias and suppressing infiltration of inflammatory cells into the CNS through a COX-2-independent mechanism. Further analysis of celecoxib-mediated suppression of EAE will help drug development for multiple sclerosis. Celecoxib is hoped to be a new choice of the treatment of multiple sclerosis.

Acknowledgement

This study was supported by the Japan Research Foundation for Clinical Pharmacology.

References

Alloza I, Baxter A, Chen Q, Matthiesen R, Vanderbroeck K. Celecoxib inhibits interleukin-12 αβ and β2 folding and secretion by a novel COX2-independent mechanism involving chaperones of the endoplasmic reticulum. Mol Pharm 2006; 69: 1579–87.

Arico S, Pattingre S, Bauvy C, Gane P, Barbat A, Codogno P, et al. Celecoxib induces apoptosis by inhibiting 3-phosphoinositide-dependent protein kinase-1 activity in the human colon cancer HT-29 cell line. J Biol Chem 2002; 277: 27613–21.

Cuzzocrea S, Mazzon E, Serraino I, Dugo L, Centorrino T, Ciccolo A, et al. Celecoxib, a selective cyclo-oxygenase-2 inhibitor reduces the severity of experimental colitis induced by dinitrobenzene sulfonic acid in rats. Eur J Pharmacol 2001; 431: 91–102.

Cuzzocrea S, Mazzon E, Sautebin L, Dugo L, Serraino I, De Sarro A, et al. Protective effects of celecoxib on lung injury and red blood cells modification induced by carrageenan in the rat. Biochem Pharmacol 2002; 63: 785–95.

Deininger MH, Schluesener HJ. Cyclooxygenases-1 and -2 are differentially localized to microglia and endothelium in rat EAE and glioma. J Neuroimmunol 1999; 95: 202–8.

Dietrich JB. The adhesion molecule ICAM-1 and its regulation in relation with the blood-brain barrier. J Neuroimmunol 2002; 128: 58–68.

Engelhardt B, Vestweber D, Hallmann R, Schulz M. E- and P-selectin are not involved in the recruitment of inflammatory cells across the blood-brain barrier in experimental autoimmune encephalomyelitis. Blood 1997; 90: 4459–72.

Grosch S, Tegeder I, Niederberger E, Brautigam L, Geisslinger G. COX-2 independent induction of cell cycle arrest and apoptosis in colon cancer cells by the selective COX-2 inhibitor celecoxib. FASEB J 2001; 15: 2742–4.

Hofmann N, Lachnit N, Streppel M, Witter B, Neiss WF, Guntinas-Lichius O, et al. Increased expression of ICAM-1, VCAM-1, MCP-1, and MIP-1 alpha by spinal perivascular macrophages during experimental allergic encephalomyelitis in rats. BMC Immunol 2002; 6: 11.

Hsu AL, Ching TT, Wang DS, Song X, Rangnekar VM, Chen CS. The cyclooxygenase-2 inhibitor celecoxib induces apoptosis by blocking Akt activation in human prostate cancer cells independently of Bcl-2. J Biol Chem 2000; 275: 11397–403.

Krakowski ML, Owens T. The central nervous system environment controls effector CD4+ T cell cytokine profile in experimental allergic encephalomyelitis. Eur J Immunol 1997; 27: 2840–7.

Kumar V, Aziz F, Sercarz E, Miller A. Regulatory T cells specific for the same framework 3 region of the Vb8.2 chain are involved in the control of collagen II-induced arthritis and experimental autoimmune encephalomyelitis. J Exp Med 1997; 185: 1725–33.

Kusunoki N, Yamazaki R, Kawai S. Induction of apoptosis in rheumatoid synovial fibroblasts by celecoxib, but not by other selective cyclooxygenase 2 inhibitors. Arthritis Rheum 2002; 46: 3159–67.

Liu X, Yue P, Zhou Z, Khuri FR, Sun SY. Death receptor regulation and celecoxib-induced apoptosis in human lung cancer cells. J Natl Cancer Inst 2004; 96: 1769–80.

Meyer F, Ramanujam KS, Gobert AP, James SP, Wilson KT. Cutting edge: cyclooxygenase-2 activation suppresses Th1 polarization in response to Helicobacter pylori. J Immunol 2003; 171: 3913–7.

Miyamoto K, Oka N, Kawasaki T, Satoi H, Akiguchi I, Kimura J. The effect of cyclooxygenase-2 inhibitor on experimental allergic neuritis. Neuroreport 1998; 9: 2331–4.

Miyamoto K, Oka N, Kawasaki T, Satoi H, Matsuo A, Akiguchi I. The action mechanism of cyclooxygenase-2 inhibitor for treatment of experimental allergic neuritis. Muscle Nerve 1999; 22: 1704–9.

Miyamoto K, Oka N, Kawasaki T, Miyake S, Yamamura T, Akiguchi I. New cyclooxygenase-2 inhibitor for treatment of experimental autoimmune neuritis. Muscle Nerve 2002; 25: 280–2.

Muthian G, Raikwar HP, Johnson C, Rajasingh J, Kalgutkar A, Marnett LJ, et al. COX-2 inhibitors modulate IL-12 signaling through JAK-STAT pathway leading to Th1 response in experimental allergic encephalomyelitis. J Clin Immunol 2006; 26: 73–85.

Nakatsuji S, Terada N, Yoshimura T, Horie Y, Furukawa M. Effects of nimesulide, a preferential cyclooxygenase-2 inhibitor, on carrageenan-induced pleurisy and stress-induced gastric lesions in rats. Prostaglandins 1996; 55: 395–402.

Nicholson LB, Kuchroo VK. Manipulation of the Th1/Th2 balance in autoimmune disease. Curr Opin Immunol 1996; 8: 837–42.

Penning TD, Talley JJ, Bertenshaw SR, Carter JS, Collins PW, Docter S, et al. Synthesis and biological evaluation of the 1,5–diarylpyrazole class of cyclooxygenase-2 inhibitors: identification of 4-[5-(4-methylphenyl)-3-(trifluoromethyl)-1H-pyrazol-1-yl]benzene sulfonamide (SC-58635, celecoxib). J Med Chem 1997; 40: 1347–65.

Prosiegel M, Neu I, Mallinger J, Wildfeuer A, Mehlber L, Vogl S, et al. Suppression of experimental autoimmune encephalomyelitis by dual cyclo-oxygenase and 5-lipoxygenase inhibition. Acta Neurol Scand 1989; 79: 223–6.

Scott GS, Kean RB, Fabis MJ, Mikheeva T, Brimer CM, Phares TW, et al. ICAM-1 upregulation in the spinal cords of PLSJL mice with experimental allergic encephalomyelitis is dependent upon TNF-alpha production triggered by the loss of blood-brain barrier integrity. J Neuroimmunol 2004; 155: 32–42.

Shishodia S, Koul D, Aggarwal BB. Cyclooxygenase (COX)-2 inhibitor celecoxib abrogates TNF-induced NF-kappa B activation through inhibition of activation of I kappa B alpha kinase and Akt in human non-small cell lung carcinoma: correlation with suppression of COX-2 synthesis. J Immunol 2004; 173: 2011–22..

Simmons RD, Hugh AR, Willenborg DO, Cowden WB. Suppression of active but not passive autoimmune encephalomyelitis by dual cyclo-oxygenase and 5-lipoxygenase inhibition. Acta Neurol Scand 1992; 85: 197–9.

Snijdewint F, Kalinski P, Wierenga E, Bos J, Kapasenberg M. Prostaglandin E2 differentially modulate cytokine secretion profiles of human T helper lymphocytes. J Immunol 1993; 150: 5321.

Vane JR, Mitchell JA, Appleton I, Tomlinson A, Bishop-Bailey D, Croxtall J, et al. Inducible isoforms of cyclooxygenase and nitric oxide synthase in inflammation. Proc Natl Acad Sci USA 1994; 91: 2046–50.

Wang K, Tarakji K, Zhou Z, Zhang M, Forudi F, Zhou X, et al. Celecoxib, a selective cyclooxygenase-2 inhibitor, decreases monocyte chemoattractant protein-1 expression and neointimal hyperplasia in the rabbit atherosclerotic balloon injury model. J Cardiovasc Pharmacol 2005; 45: 61–7.

Warner TD, Mitchell JA. Cyclooxygenases: new forms, new inhibitors, and lessons from the clinic. FASEB J 2004; 18: 790–804.

Weber F, Meyermann R, Hempel K. Experimental allergic encephalomyelitis-prophylactic and therapeutic treatment with the cyclooxygenase inhibitor piroxicam (Feldene). Int Arch Allergy Appl Immunol 1991; 95: 136–41.

Xie WL, Chipman JG, Robertson DL, Erikson RL, Simmons DL. Expression of a mitogen-responsive gene encoding prostaglandin synthase is regulated by mRNA splicing. Proc Natl Acad Sci USA 1991; 88: 2692–6.

Zhang B, Yamamura T, Kondo T, Fujiwara M, Tabira T. Regulation of experimental autoimmune encephalomyelitis by natural killer (NK) cells. J Exp Med 1997; 186: 1677–87.

The Complementarity Determining Region 2 of BV8S2 (Vβ8.2) Contributes to Antigen Recognition by Rat Invariant NKT Cell TCR[1]

Elwira Pyż,[2]* Olga Naidenko,[†] Sachiko Miyake,[‡] Takashi Yamamura,[‡] Ingolf Berberich,* Susanna Cardell,[3§] Mitchell Kronenberg,[†] and Thomas Herrmann[4]*

Invariant NKT cells (iNKT cells) are characterized by a semi-invariant TCR comprising an invariant α-chain paired with β-chains with limited BV gene usage which are specific for complexes of CD1d and glycolipid Ags like α-galactosylceramide (α-GalCer). iNKT cells can be visualized with α-GalCer-loaded CD1d tetramers, and the binding of mouse CD1d tetramers to mouse as well as to human iNKT cells suggests a high degree of conservation in recognition of glycolipid Ags between species. Surprisingly, mouse CD1d tetramers failed to stain a discrete cell population among F344/Crl rat liver lymphocytes, although comprised iNKT cells are indicated by IL-4 and IFN-γ secretion after α-GalCer stimulation. The arising hypothesis that rat iNKT TCR recognizes α-GalCer only if presented by syngeneic CD1d was then tested with the help of newly generated rat and mouse iNKT TCR-transduced cell lines. Cells expressing mouse iNKT TCR reacted to α-GalCer presented by rat or mouse CD1d and efficiently bound α-GalCer-loaded mouse CD1d tetramers. In contrast, cells expressing rat iNKT TCR responded only to α-GalCer presented by syngeneic CD1d and bound mouse CD1d tetramers only poorly or not at all. Finally, CD1d-dependent α-GalCer reactivity and binding of mouse CD1d tetramers was tested for cells expressing iNKT TCR comprising either rat or mouse AV14 (Vα14) α-chains and wild-type or mutated BV8S2 (Vβ8.2) β-chains. The results confirmed the need of syngeneic CD1d as restriction element for rat iNKT TCR and identified the CDR2 of BV8S2 as an essential site for ligand recognition by iNKT TCR. ***The Journal of Immunology,*** **2006, 176: 7447–7455.**

The hallmark of invariant NKT cells (iNKT cells)[5] is the expression of a TCR with characteristic invariant α-chain rearrangement and limited BV (Vβ) usage which recognizes glycolipids like α-galactosylceramide (α-GalCer) in a CD1d-restricted manner (1). Mouse iNKT TCR α-chains rearrange the variable gene 14 (*AV14*) and joining gene 18 (*AJ18*), which pair with β-chains of high CDR3 variability comprising BV8S2 and to lesser extent to BV7 or BV2 (2–4). The human iNKT TCR is composed of AV11/AJ18 (homolog of mouse AV14) α-chains paired with BV11 (homolog of mouse BV8) β-chains (2, 5). In the rat, homologous α-chain rearrangements have also been found (6). A contribution of iNKT cells in the control of tumors, infections, and autoimmune diseases (reviewed in Refs. 7–9) has been demonstrated in many mouse models and by clinical observations in humans.

iNKT TCR ligands are endogenous or microbial glycolipids that are presented by the nonpolymorphic MHC class I-like molecule CD1d. Crystal structures of complexes of CD1d and glycolipid Ags have been reported very recently (10–12). Natural ligands are isoglobotrihexosylceramide (13) and α-anomers of various glycosphingolipids, which have been isolated from α_4-proteobacteria (14, 15). Other ligands activate only small subpopulations of iNKT cells. Their features are reviewed in Ref. 16. Still the most thoroughly characterized Ag of iNKT cells is the α-anomer of galactosylceramide (α-GalCer), which was originally isolated from a marine sponge. Essentially all iNKT cells respond to α-GalCer, and they can be visualized with α-GalCer-loaded CD1d oligomers (reviewed in Ref. 17). Of special importance to our study is the observation that α-GalCer-loaded mouse CD1d oligomers bind to human iNKT cells (18–20) and human CD1d tetramers stain mouse iNKT cells. Thus, it appears that ligand recognition is highly conserved throughout evolution (21).

The rat also expresses genes for CD1d (22, 23) and the AV14, AJ18 (6), and BV8S2 (24) gene segments, which are highly similar to those of the mouse (>80% sequence similarity of the translated products). Peculiar to the rat is the existence of a multimember AV14 gene family and the organ-specific preferences of certain AV14AJ18 rearrangements. Within the BN/SsNHsd genome, 10 *AV14* genes have been identified (25), and analysis of F344/Crl rearrangements identified five AV14 family members, which based on CDR2 sequence similarity, have been divided into the type I and type 2 genes. Rearrangements of type I genes (*AV14S1, AV14S2, AV14S4* (a pseudogene); and *AV14S8,* described in this paper) have been reported to be predominant within intrahepatic

*Institute for Virology and Immunobiology, Würzburg University, Germany; †Division of Developmental Immunology, La Jolla Institute for Allergy and Immunology, San Diego, CA; ‡Department of Immunology, National Institute of Neuroscience, Tokyo, Japan; and §Immunology Section, Department of Cell and Molecular Biology, Lund University, Lund, Sweden

Received for publication January 3, 2006. Accepted for publication March 10, 2006.

The costs of publication of this article were defrayed in part by the payment of page charges. This article must therefore be hereby marked *advertisement* in accordance with 18 U.S.C. Section 1734 solely to indicate this fact.

[1] This work was supported by European Graduate College "Gene regulation in and by microbial pathogens" (to E.P. and T.H.) and by National Institutes of Health Grant AI 45053 (to M.K.).

[2] Current address: Institute of Infectious Disease and Molecular Medicine, Faculty of Health Sciences, Wernher and Beit Building, South Groote Schuur Campus, Observatory, 7925, Cape Town, South Africa.

[3] Current address: Department of Microbiology and Immunology, Goteborg University, Box 435, SE-405 30 Goteborg, Sweden.

[4] Address correspondence and reprint requests to Dr. Thomas Herrmann, Institut für Virologie und Immunbiologie, Versbacherstrasse 7, 97078 Würzburg, Germany. E-mail address: herrmann-t@vim.uni-wuerzburg.de

[5] Abbreviations used in this paper: iNKT cells, invariant NKT cells; α-GalCer, α-galactosylceramide; IHL, intrahepatic lymphocytes; MFI, mean fluorescence intensity.

0022-1767/06/$02.00

lymphocytes (IHL), whereas rearrangements of the type II gene *AV14S3* are more frequently found in spleen, bone marrow lymphocytes, and thymocytes (6, 25). In all cases, either a G or an A have been found at position 93, located at the VJ junction (6), which is similar to the mouse, where mostly a G but also rarely A, V, or I are found in this region (2, 26).

Despite this information on the genetics, knowledge of the phenotype, function, and Ag recognition by rat iNKT TCR-bearing cells is rather limited. The comparison of NKR-P1A-positive rat T lymphocytes (6) with mouse NKT cells has elucidated some differences in terms of phenotype and functions. First of all, NKR-P1A (rat homolog of mouse NK1.1)-positive T cells found in spleen and liver (6, 27, 28) were of CD8$\alpha\beta$ phenotype and showed no preferential BV usage. This is in stark contrast to the mouse, in which most of the NK1.1-positive T cells, and nearly all iNKT cells, are $CD4^+$ or $CD4^-CD8^-$. Secondly, NKR-P1A-positive rat T cells produce IFN-γ but not IL-4 upon in vitro CD3 stimulation (28). Thus, it appears that these cells are not the equivalent of mouse iNKT cells.

Nevertheless, there is also evidence that favors the existence of typical iNKT cells in the rat. Matsuura et al. (6) showed that coculture of F344/Crl IHL with CD1d-transduced hepatocytes leads to the accumulation of cells with AV14 transcripts, and they identified AV14AJ18 rearrangements in a NKR-$P1A^{high}$ subset of intrahepatic T lymphocytes of LEC rats (29). Additionally, another group has reported the generation of $CD4^+$ or $CD4^-CD8^-$ NKR-$P1A^+$ T cell clones from PVG rats that home to the liver and produce Th1 and Th2 cytokines (30). However, to our knowledge, α-GalCer reactivity of rat T lymphocytes or binding of α-GalCer-loaded CD1d oligomers have not been described yet. Both groups reported staining of the presumed rat iNKT cells by the BV8-specific mAb R78 (6, 30), which depending on the *Tcrb* haplotype binds to different rat homologs of mouse BV8S2. In F344/Crl rats (*Tcrb*^{a} haplotype), R78 reacts with BV8S4 (BV8S4A2) but not with BV8S2 (BV8S2A2), whereas in PVG rats (*Tcrb*^{l} haplotype) BV8S4 (BV8S4A1) is not functional and R78 Ab stains positively BV8S2 (BV8S2A1) (24, 31).

This paper describes our attempts to characterize F344/Crl rat iNKT cells, their phenotype, and their α-GalCer reactivity. Although like mouse NKT cells, the lymphocytes isolated from F344/Crl rat liver secreted cytokines upon α-GalCer in vitro stimulation, they could not bind α-GalCer-loaded mouse CD1d tetramers (mouse CD1d tetramers). To test the species specificity of recognition of α-GalCer-CD1d complexes, mouse and rat iNKT TCR were cloned, and a panel of cell lines expressing mouse and rat, wild-type or mutated iNKT TCR were generated. The $AV14^+$ lines were tested for rat vs mouse CD1d-restricted α-GalCer recognition and for binding of mouse CD1d tetramers. The results confirmed the hypothetical species specificity of CD1d-dependent α-GalCer recognition by rat iNKT cells and allowed, for the first time, definition of the important role of the CDR2β as a germline-encoded TCR region for this recognition.

Materials and Methods

Animals

C57BL/6 mice and LEW/Crl rats were bred in the animal facilities of the Institute for Virology and Immunology, University of Würzburg, Würzburg, Germany. F344/Crl rats were obtained from Charles River Wiga. All animals were maintained under specific pathogen-free conditions and were used at 6–10 wk of age.

Cell preparation and culture

Mouse and rat IHL were isolated using discontinuous Percoll (Pharmacia Biotech) gradients (40%/70% or 40%/80%) as described in Ref. 32. In both cases, liver was perfused with complete medium (via the portal vein) until it became opaque. Then the organ was homogenized by passing through a metal mesh, and cells were washed with medium. Cells were resuspended in 40% isotonic Percoll solution and underlaid with 70 or 80% isotonic Percoll solution. After 25 min of centrifugation at 900 × *g* at room temperature, mononuclear cells were isolated from the interface. Remaining erythrocytes were removed from the cell pellet by lysis with TAC buffer (Tris-ammonium chloride, 20 mM Tris (pH 7.2), 0.82% NH_4Cl). Thymocytes were isolated by passing the organ through a metal sieve followed by washing with complete medium. Primary cells and cell lines were cultured at 37°C with 5% CO_2 and H_2O-saturated atmosphere. Almost all cell types were cultured in RPMI 1640 (Invitrogen Life Technologies) supplemented with 5 or 10% FCS, 100 mM sodium pyruvate, 0.05% (w/v) glutamine, 10 mM nonessential amino acids, and 100 μM 2-ME (Invitrogen Life Technologies). DMEM with the same supplements was used for transfection of 293T cells, conducted to produce retroviruses for gene transfer.

Cloning and expression of rat and mouse iNKT TCR

Rat AV14S8 α-chain was directly cloned from F344/Crl IHL cDNA, whereas the rat AV14S1 α-chain construct was generated using molecular biology methods. For the F344/Crl AV14S8 α-chain, RNA was isolated from cytoplasmic extracts of $\sim 10^6$ IHL following the protocol of the RNeasy MiniKit (Qiagen). The cDNA was synthesized according to the manufacturer's RT-PCR protocol supplied with a First Strand cDNA Synthesis Kit (MBI Fermentas). PCR was performed with HotStar DNA polymerase (Qiagen), using AV14-specific primers: (MWG-Biotech) rVα14/1,2,3-Fow (5′-TTT GGG GCT AGG CTT CTG-3′), RCαend-STOP-Rev (5′-TCA ACT GGA CCA CAG CCT TAG CG-3′). PCR products were cloned into TOPO cloning vector (Topo pCR2.1-TOPO-TOPO TA Cloning Kit; Invitrogen Life Technologies) and sequenced using an ABI sequencer. Subsequently, rat AV14S8 α-chain DNA was ligated into *Eco*RI sites of pczCGZ5 IEGZ retroviral vector.

An AV14S1 α-chain with a V domain amino acid sequence described by Matsuura et al. (6) was generated using molecular biology methods. F344/Crl genomic DNA was amplified by PCR with rVα14-*Eco*RI-Fow (5′-GGG CTA GAA TTC TGC AGA AAA ACC ATG GGG AAG C-3′) and r/mVα14Rev (5′-CAC CAC ACA GAT GTA GGT GGC AG-3′) primers. This DNA was digested with *Eco*RI and *Esp* enzymes and gel purified. The resulting fragment, which encoded the leader and the first 72 aa of mature V region peptide, was coligated with a *EspI*-F344/Crl cDNA-*Bam*HI fragment (encoding the JC terminus of another liver-derived α-chain) into the *Eco*RI/*Bam*HI sites of pczCGZ5 IEGN vector, and the insert was sequenced. The generation of the rat BV8S2 β-chain and its mutants has been described elsewhere (33).

A mouse type 1 NKT cell TCR was cloned by RT-PCR from mouse KT12 hybridoma (34) using α-chain (mVα14-*Eco*RI-Fow: 5′-GGG GAA TTC AAC CAT GAA AAA GCG CC-3′; and mCα14-*Eco*RI-Rev: 5′-CCC GAA TTC CTC AAC TGG ACC ACA GCC-3′) and β-chain (mVβ8.2-*Bam*HI: 5′-CGG GAT CCT GAG ATG GGC TCC AGG CTC TTC-3′; and mCβend-*Bam*HI: 5′-GGG GGA TCC TCA GGA ATT TTT TTT CTT GAC C-3′)-specific primers. Mouse AV14S1A2 α-chain DNA was ligated into the *Eco*RI site of pczCGZ5 IEGN (containing genes for neomycin resistance and enhanced green fluorescence protein), and mouse BV8S2 β-chain DNA was ligated into *Bam*HI sites of pczCGZ5 IEGZ (containing genes for zeozin resistance and enhanced green fluorescence protein) retroviral vectors (35).

Rat TCR α-chains (AV14S8 and AV14S1) as well as mouse AV14SA2-TCR α-chain were expressed together with C57BL/6 mouse or rat BV8S2 TCR β-chains in BW58r/mCD28 cells using a transient three-plasmid expression system. BWr/mCD28 cells are BW58 TCR^- mouse hybridoma transduced with chimeric rat/mouse CD28 molecule (36). These cells are especially suitable for the analysis of Ag presentation by CD80-positive APC (33). Expression of transduced α-chains was estimated from the green fluorescence of the reporter gene. Cell surface expression of transduced TCR was analyzed by staining with anti-mouse CD3 mAb. When necessary to obtain similar levels of TCR expression, cell lines were sorted using a FACSVantage (BD Biosciences) machine or by coculture in selection medium containing 1 mg/ml neomycin (Invitrogen Life Technologies) or 250 μg/ml zeozin (CAYLA), alternatively.

Cloning and expression of rat and mouse CD1d

P80rCD80 cells were transduced with mouse or rat CD1d. P80rCD80 cells are P80 cells (P815 mouse mastocytoma transduced with rat CD80; Ref. 37) which, to increase rat CD80 expression, were additionally infected with pczCGZ5IZ or pczCGZ5IEGZ retroviral vectors expressing genes for rat CD80 and zeozin resistance. These have been generated by RT-PCR from the CD80-containing BCMGSC vector (37) and subsequently cloned into the *Eco*RI sites of both retroviral vectors. P80rCD80 cells transduced with

rat CD1d are designated as P80rCD80rCD1d, those transduced with mouse CD1d as P80rCD80mCD1d.

Mouse CD1d was cloned from A20mCD1d cell line (38) by RT-PCR using the following primers: mCD1d-*Eco*RI-Fow (5'-GGG GAG AAT TCC GGC GCT ATG CGG TAC CTA CC-3'); and mCD1d-*Eco*RI-Rev (5'-GGT GGA ATT CAG AGT CAC CGG ATG TCT TGA TAA G-3'). The sequence of the insert showed a complete overlap with the mouse CD1d sequence available in the gene bank under X13170 (39). Rat CD1d cDNA was obtained by RT-PCR using RNA isolated from F344/Crl rat bone marrow as a template and CD1d-specific primers: N366 (5'-TCG GAG CCC AGG GCT GTG TAG A-3'); and rCD1dRev (5'-TTC TGA GCA GAC AAG GAC TGA-3'). PCR product was cloned into TOPO cloning vector and sequenced. The sequence was identical with rat CD1d (GenBank accession number AB029486) published by Katabami et al. (23). Mouse and rat CD1d DNA were cloned into *Eco*RI site of pczCGZ5IZ and pczCGZ5 IEGZ vectors, respectively, and were further used for retroviral infection of P80rCD80 cells.

The expression of mouse CD1d was tested with the CD1d-specific mAb 1B1 (BD Pharmingen), whereas expression of rat CD1d was assessed from the green fluorescence of the *EGFP* reporter gene. Surface expression of rat CD1d was also confirmed with a novel rat CD1d-specific mAb (E. Pyz and T. Herrmann, unpublished observations). The Ag-presenting cell lines were enriched for CD1d expression by cell sorting or selection with antibiotics.

Stimulation with α-GalCer in vitro

α-GalCer was generated as described (40). The reactivity of mouse and rat IHLs to α-GalCer was tested by culture of IHL (1×10^5 cells/well of a 96-well round-bottom plate) in the presence of α-GalCer (100 ng/ml), vehicle (DMSO), or complete medium for 24 h at 37°C. The level of IL-4 and IFN-γ released into culture supernatants was determined using ELISA kits (BD Pharmingen).

To analyze the α-GalCer reactivity of TCR-transduced cell lines, mouse and rat thymocytes (1×10^6 cells/well), or CD1d-transduced cells (P80mCD1drCD80, P80rCD1drCD80, 5×10^4 cell/well) used as APC were loaded with either α-GalCer (1–100 ng/ml) or vehicle (DMSO) for 1–2 h before the addition of responder cells. As a positive control, TCR-positive cell lines were stimulated with plate-bound anti-mouse CD3 mAb 145C11. After 24 h of culture, supernatants were taken, and the secreted mouse IL-2 was quantified using a commercial ELISA Kit (BD Pharmingen).

Immunofluorescence and flow cytometry

For the staining, 2×10^5 cells were diluted in 100 μl of FACS buffer (PBS (pH7.4), 0.1% BSA, 0.02% NaN_3) and were treated for 10 min at 4°C with normal mouse Ig (Sigma-Aldrich) or mouse FcγR-specific 2.4G2 Ab to block unspecific binding or binding to Fc receptors. Subsequently, cells were stained for 30 min with labeled mAbs, washed, and stained with another mAb or analyzed with a FACScan or FACSCalibur flow cytometer (BD Biosciences).

All mouse and rat mAbs were obtained from BD Pharmingen and are given with their clone names: mouse Vβ8.1, 8.2, 8.3 (F23.1); mouse CD3 ε-chain (145-C11); mouse CD1d (1B1); mouse CD4 (GK1.5); mouse CD8α (53-6.7); NK1.1 (PK136); BV8S4A1 and BV8S4A2, Vβ8.2 of LEW rats and Vβ8.4 of F344/Crl rat (R78); rat TCR β-chain (R73); rat CD4 (W3/25); rat CD4 (OX35); rat CD8β (3.4.1.); rat NKR-P1A (10-78). Abs were usually FITC or PE labeled. Biotinylated mAbs, when used, were visualized with streptavidin-CyChrome. Unconjugated Abs, used in indirect immunofluorescent staining, were detected by using fluorochrome-conjugated Abs: PE- or Cy5.5-conjugated $(Fab')_2$ fragment of donkey anti-mouse IgG or goat anti-hamster IgG FITC obtained from Dianova or Serotec).

Staining with α-GalCer-loaded mouse CD1d-PE tetramer

α-GalCer-loaded or control mouse CD1d-PE tetramers were generated as described in Ref. 18. Tetramer staining of mouse/rat IHL- or TCR-transduced cell lines was performed as normal FACS staining, but with incubation for 1 h at room temperature. Tetramer concentrations were 350 (high tetramer) or 35 ng/50 μl cell suspension (low tetramer).

Results

Phenotype and α-GalCer response of rat IHL

In mouse and human, the highest proportion iNKT cells can be found among intrahepatic lymphocytes. In an attempt to identify the corresponding population in rat, IHL of F344/Crl rats and C57BL/6 mice were compared for cell surface phenotype (Fig. 1*A*), binding of α-Gal-loaded mouse CD1d tetramers (Fig. 1*B*), and α-GalCer-induced cytokine production (Fig. 1*C*). In agreement with published data, about one-third of mouse IHL coexpressed NK1.1 (mouse homolog to rat NKR-P1A) and TCR. More than 20% of IHL coexpressed NK1.1 and CD4, but very few coexpressed NK1.1 and CD8αβ. As shown in Fig. 1*B*, ~27% of IHL show costaining of α-GalCer-loaded CD1d tetramer and anti-CD3, with the tetramer positive cells having a lower or intermediate level of expression of CD3. 25.5% of IHL were costained by tetramer and anti-NK1.1 (data not shown) and 20.4% by tetramer and anti-CD4, whereas only very few (0.38%) stained with CD1d tetramer and CD8-specific mAb (data not shown).

The phenotypes of rat and mouse IHL differed considerably. First of all, <5% of rat IHL coexpressed NKR-P1A and CD3, and most of these cells were positive for CD8αβ but not for CD4, and they did not express intermediate CD3 levels. Secondly, in contrast to results found in mice, only a very small number of $CD3^+$ rat IHL were stained with α-GalCer-loaded mouse CD1d tetramer;

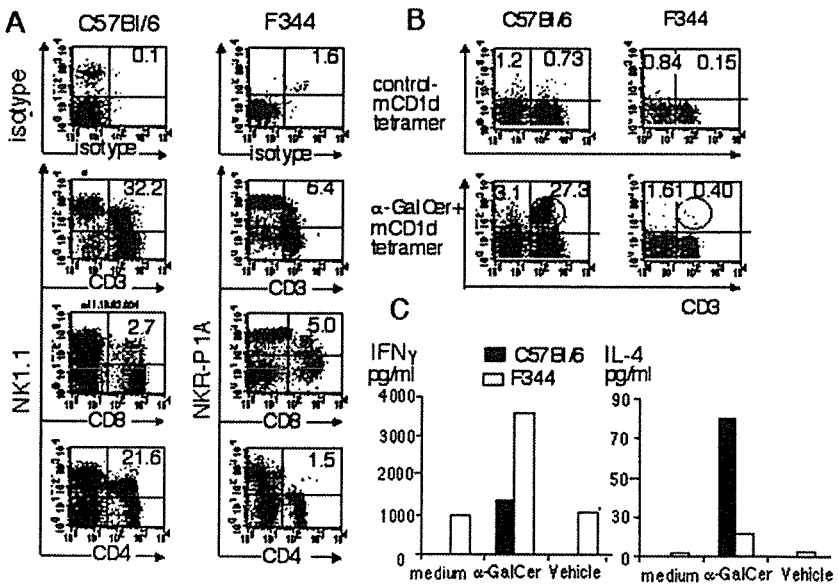

FIGURE 1. Phenotypic and functional analysis of typical iNKT cell features of C57BL/6 mouse and F344/Crl rat IHL. *A*, Two-color flow cytometry for coexpression of NK1.1 or NKR-P1A and indicated T cell markers. Percent of positive cells are indicated by numbers in the *upper right quadrant*. *B*, Two-color flow cytometry for binding of α-GalCer-loaded or unloaded mouse CD1d tetramers to $CD3^+$ positive (*upper right quadrant*) or $CD3^-$ (*upper left quadrant*) C57BL/6 mouse or F344/Crl rat IHL. Percentages of tetramer-positive cells are given in the respective quadrants. *C*, IFN-γ or IL-4 secretion during 24-h stimulation of 1×10^5 rat or mouse IHL with 100 ng/ml α-GalCer dissolved in DMSO, vehicle (DMSO alone), or medium alone. *Ordinate*, Cytokine concentration in picograms per milliliter.

0.4% of IHL were stained with α-GalCer-loaded tetramer and 0.15% with control tetramer. Even higher proportions of $CD3^-$ lymphocytes were stained by α-GalCer-loaded tetramers (1.61%) or control tetramers (0.84%), which made it likely that (much of) the tetramer staining of $CD3^+$ rat IHL was unspecific.

To test whether the lack of binding of mouse CD1d tetramer to rat IHL was due to the absence of α-GalCer-specific cells in F344/Crl rat liver, the α-GalCer reactivity of F344/Crl and C57BL/6 IHL (Fig. 1*C*) was compared. After 24 h of stimulation with α-GalCer (100 ng/ml), mouse and rat liver lymphocytes produced both IFN-γ and IL-4. The amount of rat IL-4 reached ~15% of that secreted by mouse cells. The IFN-γ production by rat IHL exceeded that of mouse IHL, but rat IHL showed also a high level of background IFN-γ production.

The α-GalCer-induced activation of cytokine production in conjunction with the detection of AV14AJ18 rearrangements in rat IHL strongly support the existence of an iNKT cell population in F344/Crl rats, although these cells could not be detected by mouse CD1d tetramer. This could be a consequence of 1) an extremely low frequency of rat iNKT cells and/or 2) a requirement for presentation of α-GalCer by syngeneic CD1d (species specificity), which finally would result in a lack of binding of mouse CD1d tetramers to rat iNKT TCR. To test the latter hypothesis, iNKT TCRs were cloned and expressed in TCR-negative BW58r/mCD28 cells and tested for mouse CD1d tetramer binding. In addition, these lines as well as lines expressing iNKT TCR variants were tested for reactivity to α-GalCer presented by mouse or rat CD1d.

Cloning and transduction of mouse and rat CD1d and iNKT TCR

Cloning, transduction, and quantification of surface expression of iNKT TCR was performed as described in *Materials and Methods*. Three AV14 α-chains were cloned into a retroviral vector carrying an *EGFP* as reporter gene. Two of them comprised V-encoded amino acid sequences identical with that of rat AV14S1 and rat AV14S8. The mouse AV14S1A2-chain was cloned from the α-GalCer-reactive mouse C57BL/6-derived iNKT cell hybridoma KT12. All AV14 α-chains were coexpressed with different mouse or rat BV8S2 β-chains, the properties of which will be discussed later in this section.

The sequences of the tested iNKT TCR α-chains are compared in the upper part of Fig. 2. Both rat AV14S1 and rat AV14S8 α-chain comprise type 1 AV14 sequences. The V domain of the rat AV14S1 α-chain is identical with sequences previously found by Matsuura et al. in F344/Crl rat liver (6). The rat AV14S8 α-chain sequence was directly cloned from F344/Crl IHL, as described in *Materials and Methods*. AV14S8 has not yet been described for F344/Crl rats, but an identical sequence has been found in the BN/SsNHsd rat genome, where it has been named AV14S8 (25). A peculiarity of the AV14S8-comprising α-chain used in this study may be the valine located at position 93 of the VJ junction which corresponds to the adult type of AV14AJ18 rearrangements (26). Otherwise, the mature Vα domains of the two rat TCRs differed by the following substitutions: K1R, Q15E, and K51T.

The middle part of Fig. 2 aligns the sequences of the TCR β-chains used in this study. The BV8S2-positive mouse β-chain was originally isolated from the iNKT T cell hybridoma KT12. The rat BV8S2 (BV8S2A1 or Tcrb-V8.2^1)-comprising β-chain used in this study was derived from the rat T cell hybridoma 35/1, which was generated with an encephalitogenic cell line of LEW/Crl origin as fusion partner. The 35/1 TCR is $RT1B^1$-restricted $gpMBP_{68-88}$ specific and reacts also with the superantigens of *Yersinia pseudotuberculosis* and *Mycoplasma arthritidis* and the staphylococcal enterotoxins B and C1 (33). As previously described in some detail (33), replacement of the CDR2 and/or the CDR4/HV4 of the BV8S4A2 with those of F344/Crl rats had distinct effects on (super)Ag reactivity. Changes in the CDR2 abolished reactivity for peptide Ag and staphylococcal enterotoxins B and C1, whereas mutation of the HV4/CDR4 affected only the response to staphylococcal enterotoxins (33). The β-chain containing the mutations within CDR2 and CDR4 is, with exception of a lacking L14K substitution, identical with the BV8S4A2 of F344/Crl rats. It lost specificity for the peptide Ag, staphylococcal enterotoxins and the superantigen of *M. arthritidis* (33).

The lower part of Fig. 2 presents the amino acid sequence of the α-1 and α-2 domains of rat and mouse CD1d. The α-helical parts

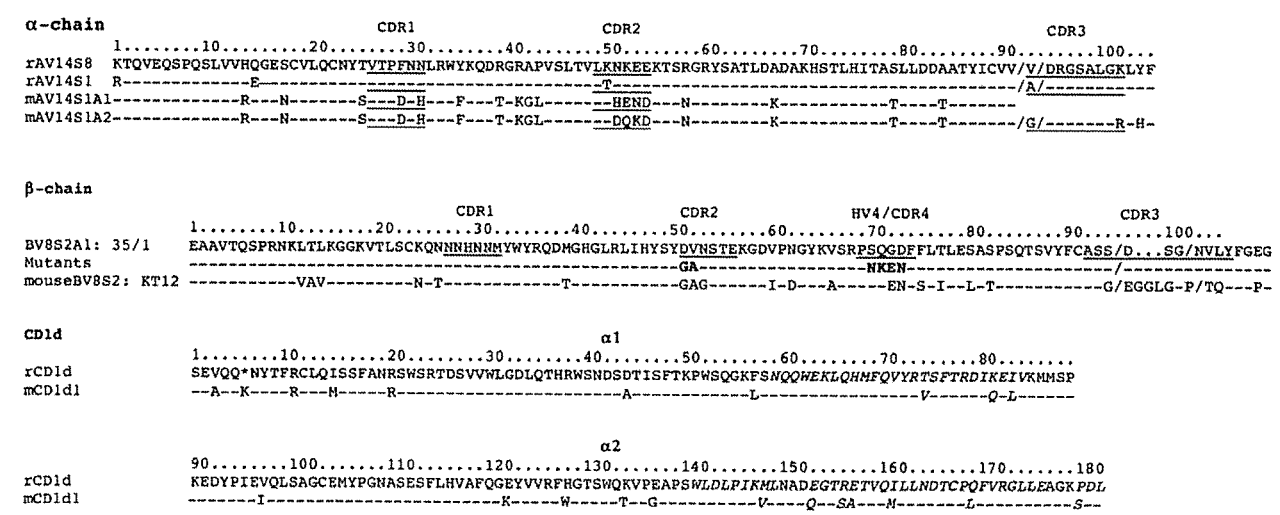

FIGURE 2. Alignment of amino acid sequences of the mature peptides TCR chain proteins (α-chain and β-chain) and CD1d molecules used or discussed in this study. Underlined parts of the TCR sequences indicate localization of CDRs. Parts of CD1d sequences in italics indicate α-helical regions. Amino acid sequences were deduced from the nucleotide sequences, the accession numbers of which can be found in GenBank: rAV14S8 α-chain, DQ340291; rAV14S1 α-chain, DQ340293; mAV14S1, AY158221; mAV14S1A2 (KT12 hybridoma), DQ340292; BV8S2A1 TCR35/1 β-chain, AY228549. Mutants entry indicates localization of the CDR2 and CDR4/HV4 substitutions introduced in the TCR35/1 β-chain, which are highlighted by bold letters. mBV8S2 TCR KT12, DQ340294; mCD1d (mouse CD1d), X13170.1; rCD1d (rat CD1d), AB029486.

of CD1d are marked. The α helices of the α1 domains differ in 3 aa. Visualization of the of the PDB files 1ZHN (10) and 1Z5L (12) of the mouse CD1d crystal structure by Swiss-PDB-viewer (http://swissmodel.expasy.org/SM_TOPPAGE.html) shows that T74 points upwards and K81 outwards, defining them as theoretical contact sites with the TCR. I83 points into the binding groove. The α-helical parts of the α-2 domain differ by 7 aa. With exception of the R157S, side chains of all substitutions show upwards and provide possible contacts for the TCR. In contrast to the differences in potential TCR contacts, those amino acids shown to provide H bonds with α-GalCer are conserved (12). Both *CD1d* genes were expressed in P815 cells (P80rCD80) overexpressing rat CD80 as described in *Materials and Methods.*

Species specificity of CD1d restriction in Ag recognition by rat iNKT TCR

First, we tested three responder cell lines for their α-GalCer reactivity and their capacity to bind mouse CD1d tetramers. The lines were BWr/mCD28 cells expressing: 1) as positive control, mouse iNKT TCR isolated from the KT12 hybridoma which consisted of a mouse AV14S1A2 α-chain and mouse BV8S2 β-chain; 2) rat AV14S1 α-chain with the CDR2+4 β-chain mutant; 3) the rat AV14S8 α-chain with the same β-chain mutant. The BV8S4-like CDR2+4 β-chain mutant was used, because there is circumstantial evidence that in F344/Crl rats, iNKT cells express the BV8S4-comprising β-chains (6). The two rat TCR lines expressed very similar levels of TCR, whereas expression of the mouse TCR was considerably lower (Fig. 3). Cell lines were tested three to five times for their α-GalCer-induced IL-2 secretion. IL-2 levels after CD3 ligation were quite similar, with the exception of sometimes considerably lower IL-2 production by the mouse iNKT TCR-transduced line (data not shown). Fig. 3 shows data from one representative assay of α-GalCer-induced IL-2 secretion. The APC-type thymocytes vs CD1d-transduced P80 cells and the origin of the transduced CD1d (rat vs mouse) considerably affected the outcome of the assay. Generally, with CD1d-transduced P80rCD80 cells as APC, Il-2 production was much higher than with thymocytes. This may reflect the differences in the level of CD1d and CD80 surface expression in primary vs CD1d-transduced cells (data not shown). In assays with mouse thymocytes as APC, some background IL-2 production was found, even if TCR-negative BW58 cells were used as responders, suggesting that IL-2 was secreted by α-GalCer-stimulated thymocytes (Figs. 3 and 5). With regard to a possible species specificity in CD1d-restricted α-GalCer recognition, all three lines responded to α-GalCer presented by rat CD1d-expressing cells, whereas α-GalCer mouse CD1d complexes stimulated only mouse iNKT TCR responder cells. In addition, the stimulation of the line expressing the rat AV14S1 α-chain was considerably stronger than of the rat AV14S8 α-chain-expressing line.

The differences in the response to α-GalCer presented by mouse CD1d correlated with the pattern of mouse CD1d tetramer staining as is shown in Fig. 3 Binding of mouse CD1d tetramers was normalized by dividing mean fluorescence intensity (MFI) of tetramer staining, through MFI of CD3 staining. After normalization, tetramer staining of the mouse iNKT TCR-expressing line was 24-fold, respectively, 8-fold stronger than that of the rat AV14S8 α-chain-expressing line or the rat AV14S1 α-chain-expressing line.

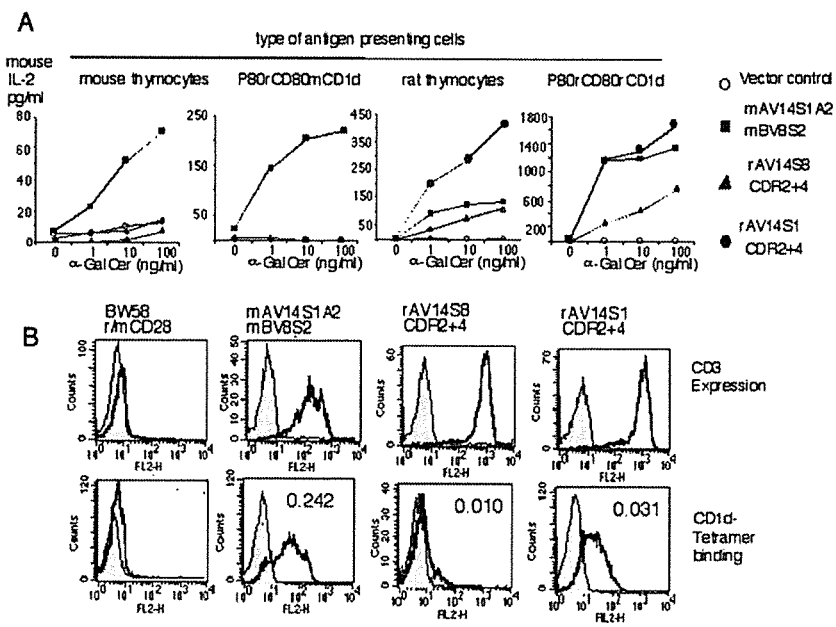

FIGURE 3. *A*, Species specificity of CD1d-restricted α-GalCer recognition by rat iNKT TCR-transduced cells. The graphs in the upper row indicate degree of IL-2 production (please note the different scales of the ordinates) by TCR-transduced BW58r/mCD28 cells after stimulation with α-GalCer presented by different APC-expressing mouse or rat CD1d. Transduced TCR: ○, vector control; ■, mAV14S1A2+mBV8S2 (mouse α-chain + mouse β-chain); ▲, AV14S8 + rat CDR2+4 β-chain (rat AVS8 α-chain + BV8S4-like rat β-chain); ●, AV14S1 + rat CDR2+4 β-chain (rat AVS1 α-chain + BV8S4-like rat β-chain). Amino acid sequences of the TCR chains used by these are given in Fig. 2. The type of α-GalCer-presenting cells and concentrations of α-GalCer used for stimulation are indicated on top of the respective graphs and at the abscissa, respectively. Zero ng/ml indicates the use of vehicle control. *B, Upper row*, CD3 expression of TCR-transduced cell lines used in *A*. Binding of isotype control (▨) or anti-CD3 (□). *Lower row*, Mouse CD1d tetramer staining. Binding of unloaded control (350 ng/50 μl sample, ▨) and of α-GalCer-loaded tetramers (350 ng/50-μl sample, □). The type of transduced TCR is given on top of the histograms. The numbers in the histogram give ratios of MFIs for staining with α-GalCer-loaded mouse CD1d tetramers divided by that for staining with anti-CD3.

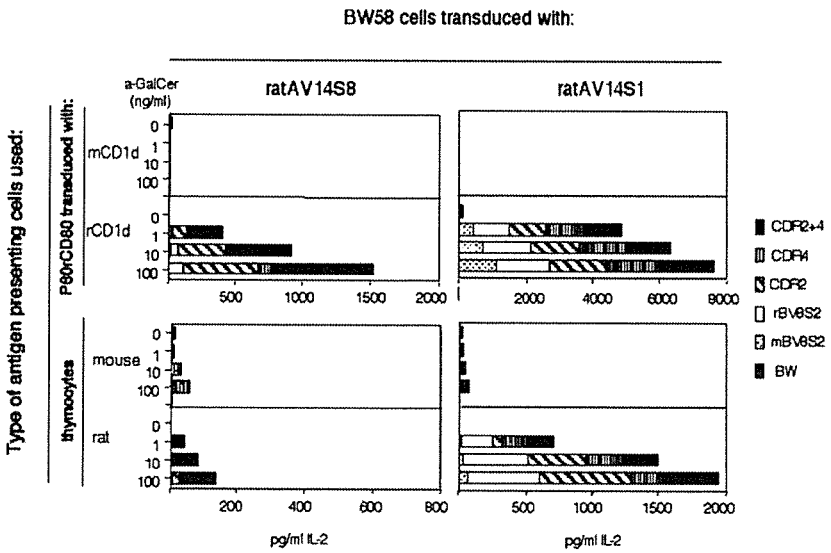

FIGURE 4. CD1d-restricted α-GalCer recognition of rat iNKT TCR. Species specificity of CD1d restriction. Shown is the α-GalCer-induced IL-2 production of BW58r/m CD28 transduced with rat AV14S1 or AV148 α-chains and various β-chains and different types of APC. Each section of the column indicates IL-2 production by cells expressing a certain α-β-chain combination. The α-chain is indicated at the top of the graph, the β-chains are indicated by the symbols in the graph. BW, Cells transduced with vector control. Ordinate, Type of APCs and the origin of CD1d. Note the variation of the scales indicating IL-2 production in the various graphs. α-GalCer concentrations are given in nanograms per milliliter. Vehicle designates culture with solvent (DMSO) only.

Effects of iNKT TCR α- and β-chain differences on CD1d-restricted α-GalCer recognition

We have previously analyzed the effects of CDR2 and/or CDR4 mutations of rat BV8S2 on the recognition of peptide Ags and superantigens (33). To learn whether the known BV encoded (super)Ag recognition sites may also contribute to α-GalCer recognition, AV14 α-chains were coexpressed with the various rat BV8S2 β-chain mutants and a mouse BV8S2 β-chain. These lines were then tested for the response to α-GalCer presented either by rat or mouse CD1d and for binding of α-GalCer-loaded mouse CD1d tetramer.

All lines expressed similar levels of TCR (summarized in Fig. 6) and produced similar amounts of IL-2 after stimulation with anti-CD3 mAb, with the exception of the mouse β-chain-expressing lines, which sometimes showed a rather low level of IL-2 production (data not shown). All lines were tested two to five times; and although the overall degree of stimulation varied between experiments, the patterns of α-GalCer reactivity remained the same. Figs. 4 and 5 show results from a representative experiment comparing all cell lines and Fig. 6 summarizes the results of all experiments.

The iNKT TCR composition affected the α-GalCer reactivity as follows: 1) the α-chain sequence of the transduced TCR largely affected the general degree of α-GalCer reactivity, because all rat AV14S1 α-chain-expressing lines responded considerably better to α-GalCer than the corresponding rat AV14S8 α-chain-expressing lines (Figs. 3 and 4); 2) lines with TCR comprising the two rat α-chains showed no or only a marginal response to α-GalCer which was presented by mouse CD1d, regardless of the type of the pairing β-chain (Fig. 4). These findings confirmed and extended the results on the species specificity of CD1d-restricted α-GalCer recognition by rat iNKT TCR shown in Fig. 3) only lines with TCR comprising the mouse α-chain in combination with mouse β-chain or with suitable rat β-chains responded to α-GalCer presented by mouse CD1d (Fig. 5). Suitable were those rat β-chains, which contained the BV8S4-like CDR2 (CDR2 or CDR2+4 mutant), whereas β-chains with the CDR2 of rat BV8S2 (CDR4 mutant and wild-type BV8S2) showed in the same setting only a marginal or no response. This pattern of reactivity maps the CDR2 of the β-chain as a region contributing to CD1d-restricted α-GalCer recognition in the interspecies comparison.

In contrast to the variation in the response to α-GalCer presented by mouse CD1d, recognition of rat CD1d-α-GalCer complexes was largely unaffected by the β-chain of iNKT TCR. All lines expressing TCR comprising the rat or mouse AV14S1 α-chains (Figs. 4 and 5) showed a very similar response. The

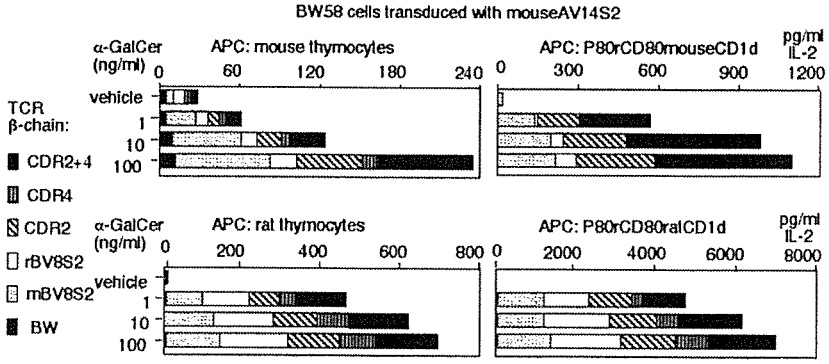

FIGURE 5. Analysis of mouse CD1d restricted α -GalCer recognition by chimeric mouse α- rat-β-chain iNKT TCR reveals contribution of CDR2β to ligand recognition by iNKT TCR. Shown is IL-2 production of BW58r/m CD28 transduced with AV14S1A2 α-chains and various β-chains indicated by the symbols in the graph to α-GalCer presented by indicated APC. BW indicates cells transduced with vector control. Every section of the columns indicates IL-2 production by cells expressing a certain α-β-chain combination. Note the variation of the scales indicating IL-2 production in the various graphs. α-GalCer concentrations are given in ng/ml. Vehicle designates culture with solvent (DMSO) only.